



## RECENT DEVELOPMENTS IN THE FIELD-BOUNDARY ELEMENT METHOD FOR FINITE/SMALL STRAIN ELASTOPLASTICITY

HIROSHI OKADA and SATYA N. ATLURI

Computational Mechanics Center, Georgia Institute of Technology, Atlanta,  
 Georgia 30332-0356, U.S.A.

**Abstract**—In this paper, some recent works of the authors, in the area of the field-boundary element method for finite/small strain elastoplasticity [Okada, Rajiyah and Atluri (1988a) *J. Appl. Mech.* **55**, 786–794; (1988b) *Comput. Struct.* **30**, 275–288; (1989) *Comput. Mech.* **4**, 165–175; (1990) *Int. J. Numer. Meth. Engng* **29**, 15–35], are summarized. Certain new integral representations for displacement (velocity) gradients, which are derived recently by the authors using the weighted residual method, are presented. Early formulations for boundary element methods for linear elasticity and small strain elastoplasticity [see Banerjee and Butterfield (1981) *Boundary Element Methods in Engineering Science*. McGraw-Hill; Banerjee and Cathie (1980) *Int. J. Mech. Sci.* **22**, 233–245; Banerjee and Raveendra (1986) *Int. J. Numer. Meth. Engng* **23**, 985–1002; (1987) *J. Engng Mech.* **113**, 252–265; Brebbia (1978) *The Boundary Element Method in Engineering*. Pentech Press; Chandra and Mukherjee (1983) *J. Strain Anal.* **18**, 261–270; Cruse (1969) *Int. J. Solids Structures* **5**, 1259–1274; Mukherjee and Chandra (1987) *Boundary Element Methods in Mechanics*, Elsevier Science Publishers; Mukherjee and Kumar (1978) *ASME J. Appl. Mech.* **45**, 785–790; Rizzo (1967) *Q. Appl. Math.* **25**, 83–95; Swedlow and Cruse (1971) *Int. J. Solids Structures* **7**, 1673–1683] are also shown along with these new integral equation representations. These new integral representations have lower order singularities, as compared to those that are obtained by a direct differentiation of the integral representations for displacement (velocity). They are quite attractive from a numerical analysis point of view, and enable the evaluation of the gradients at the boundary of the body, without any difficulties of hyper-singularities as in the conventional approach. In this new approach, the integrals, which have the highest order of the singularity, are evaluated in the sense of Cauchy principal value. Stresses and strains can be obtained directly at the boundary, using these new integral representations, whereas alternate methods or special regularization techniques† are required when the conventional type integral equation for the gradients is used. These new integral equations can unify the methods of obtaining stresses as well as strains at the interior and at the boundary of the body. As shown in this article, this is very advantageous in applications to small and finite strain elastoplasticity. The third topic in this paper is a new field-boundary element method for the analysis of a class of problems of finite strain elastoplasticity, that involve bifurcation phenomena in the solution path, such as the buckling of a beam-column, diffused necking of a tensile bar, etc. The field-boundary element method is especially advantageous in the application to the large strain elastoplasticity, since the formulation can cope with the incompressibility of the material in the regime of fully developed plastic flow. This is not true in the case of the finite element displacement method. A full tangent stiffness method has been proposed by the authors to solve such classes of problems. This formulation accounts for all the non-linearities in the problem, and allows for the calculation of the displacement field directly. The problem of diffused necking of a tensile plate is solved for illustrative purposes. It is clearly seen that the full tangent stiffness field-boundary element method is capable not only of capturing the diffused necking bifurcation but also of analysing the post bifurcation diffused necking solution.

### 1. NONHYPER-SINGULAR INTEGRAL REPRESENTATIONS FOR VELOCITY (DISPLACEMENT) GRADIENTS IN ELASTIC-PLASTIC SOLIDS (SMALL OR FINITE DEFORMATIONS)

Integral representations for displacement (velocity) gradients in elastic or elastic-plastic solids undergoing small or large deformations are presented. Compared to the cases wherein direct differentiation of the integral representations for displacements (or velocities) were carried out to obtain velocity gradients, the present integral representations have lower order singularities which are quite tractable from a numerical evaluation point of view. Moreover, the present representations allow the source point to be taken, in the limit, to

† See Krishnasamy *et al.* (1991), for the regularization techniques in the hyper-singular integral equations.

the boundary, without any difficulties. This obviates the need for a two tier system of evaluation of deformation gradients in the interior of the domain, and at the boundary of the domain. It is expected that the present formulations would yield more accurate and stable deformation gradients in problems dominated by geometric and material nonlinearities. This section deals with velocity gradient representations for four different cases of practical interest: (i) infinitesimal deformation of a linear elastic solid; (ii) small strain elastoplastic behavior; (iii) finite strain elastoplastic behavior; (iv) large deformation behavior of a semi-linear elastic solid, involving a linear relation between the second Piola–Kirchhoff stress and the Green–Lagrange strain. In case (iii), an updated Lagrangian formulation is used, whereas, in case (iv), a total Lagrangian approach is used.

All the singular integral representations described in this section are evaluated in the sense of Cauchy principal values. Hence, residual or jump terms arise out of these singular integrals. The jump terms, which arise from some generic terms which appear in the integral equations for velocity gradients, are discussed in the context of finite strain elastoplasticity. Numerical examples are provided for the problems of small and finite strain elastoplasticity, along with the detailed schemes for the evaluation of singular integrals and for the incremental calculation of elastoplasticity. It is demonstrated that the BEM formulation with the nonhyper-singular integral equation tends to give a superior numerical reliability in the calculations of finite and small strain elastoplasticity.

1.1. *Infinitesimal deformation of a linear elastic solid*

Let  $\sigma_{ij}$  be the Cartesian components of the Cauchy stress tensor, and let  $f_i$  be the body force per unit volume. The equations of linear and angular momentum balance are:

$$\sigma_{j,i,j} + f_i = 0, \tag{1}$$

$$\sigma_{ij} = \sigma_{ji}, \tag{2}$$

where  $(\ )_{,i}$  denotes differentiation with respect to material coordinates  $x_i$ . For a linear elastic isotropic solid, the stress–strain relations are:

$$\sigma_{ij} = E_{ijkl}\epsilon_{kl}, \tag{3}$$

$$E_{ijmn} = \lambda\delta_{ij}\delta_{mn} + \mu(\delta_{im}\delta_{jn} + \delta_{in}\delta_{jm}), \tag{4}$$

where,  $\lambda$  and  $\mu$  are Lamé constants and  $\delta_{ij}$  the Kronecker delta. The strain–displacement relations are

$$\epsilon_{kl} = \frac{1}{2}(u_{k,l} + u_{l,k}). \tag{5}$$

The boundary tractions, are given by:

$$t_j = n_i\sigma_{ij}, \tag{6}$$

where  $n_i$  are components of a unit outward normal to the boundary  $\partial\Omega$ .

Let  $u_i$  be the trial functions for displacements, and let  $\bar{u}_i$  be the test functions. The weak-forms of the equilibrium equation (1), can be written as:

$$\int_{\Omega} (\sigma_{j,i,j} + f_i)\bar{u}_i \, d\Omega = 0, \tag{7}$$

where  $\sigma_{ij}$  are assumed to be written as functions of  $u_i$  through eqns (3) and (4).

We assume that the test functions  $\bar{u}_i$  are the fundamental solutions, in infinite space, to the Navier equations, i.e.

$$[E_{ijkl}\bar{u}_{k,l}]_{,i} + \delta(x_m - \xi_m)\delta_{jp}e_p = 0, \tag{8}$$

where  $e_p$  denotes the direction of the unit load at  $x_m = \xi_m$ . We assume that the solid is isotropic, in which case the solution  $\bar{u}_i$  for (8) is readily available. Thus,

$$\bar{u}_j = u_{jp}^* e_p \quad (\text{no sum for } p) \tag{9}$$

and

$$\bar{t}_j = t_{jp}^* e_p \equiv n_i E_{ijkl} (u_{kp,l}^*). \tag{10}$$

Here,  $u_{jp}^*$  is the  $j$ th component of displacement at location  $x_m$  due to a unit load along the  $p$ th direction at the location  $\xi_m$ . Likewise,  $t_{jp}^*$  is the  $j$ th component of traction on an oriented surface at  $x_m$  due to a unit load along the  $p$ th direction at  $\xi_m$ . By using the divergence theorem twice on eqn (7), and substituting eqn (8) in the resulting equation, one obtains the integral equation :

$$u_p(\xi_m) = \int_{\partial\Omega} [t_j(x_m) u_{jp}^*(x_m, \xi_m) - u_j(x_m) t_{jp}^*(x_m, \xi_m)] d\partial\Omega + \int_{\Omega} f_j(x_m) u_{jp}^*(x_m, \xi_m) d\Omega. \tag{11}$$

By taking the point  $\xi_m$ , in the limit, to the boundary, one may obtain the well-known boundary integral equations for  $u_p$ . It is also well-known, that the singular kernels  $u_{jp}^*$  and  $t_{jp}^*$  remain integrable in the limit when  $\xi_m$  tends to the boundary. By a direct differentiation of eqn (11) with respect to  $\xi_m$ , one may obtain :

$$u_{p,k}(\xi_m) = \int_{\partial\Omega} \left[ t_j(x_m) \frac{\partial u_{jp}^*(x_m, \xi_m)}{\partial \xi_k} - u_j(x_m) \frac{\partial t_{jp}^*(x_m, \xi_m)}{\partial \xi_k} \right] d\partial\Omega + \int_{\Omega} f_j(x_m) \frac{\partial u_{jp}^*(x_m, \xi_m)}{\partial \xi_k} d\Omega. \tag{12}$$

In the limit as  $\xi_m \rightarrow \partial\Omega$ , the kernel  $\partial t_{jp}^*/\partial \xi_k$  becomes hyper-singular, and becomes numerically intractable. It is with the aim of circumventing these difficulties, that the present alternate types of integral representation for displacement gradients are directly developed.

Instead of writing the weak-form of the linear momentum balance relations in a single scalar-form as in eqn (7), we write the weak-forms of the linear momentum balance relation in a three component vector form, as :

$$\int_{\Omega} (\sigma_{ij,i} + f_j) \bar{u}_{j,k} d\Omega = 0. \tag{13}$$

In eqn (13),  $( )_{,i}$  implies  $\partial( )/\partial x_i$ . Assuming that the linear elastic solid is homogeneous, we rewrite (13) as :

$$\int_{\Omega} [E_{ijmn} u_{m,ni} + f_j] \bar{u}_{j,k} d\Omega = 0. \tag{14}$$

Integrating eqn (14) by parts, applying the divergence theorem three times, and making use of eqn (6), one obtains :

$$\int_{\partial\Omega} (t_j \bar{u}_{j,k} + \bar{t}_m u_{m,k} - n_k E_{ijmn} u_{m,n} \bar{u}_{j,i}) d\partial\Omega + \int_{\Omega} \bar{f}_m u_{m,k} d\Omega + \int_{\Omega} f_j \bar{u}_{j,k} d\Omega = 0. \tag{15}$$

Here

$$\bar{f}_j = -(E_{ijkl} \bar{u}_{k,l})_{,i} \tag{16}$$

and

$$\bar{t}_m = E_{ijmn}\bar{u}_{j,i}n_m. \tag{17}$$

Upon taking  $\bar{u}_i$  and  $\bar{t}_i$  to be as in eqns (8, 9 and 10), one obtains the integral relation :

$$Cu_{p,k}(\xi_m) = \int_{\partial\Omega} (n_k E_{ijmn} u_{m,n} u_{jp,i}^* - t_j u_{jp,k}^* - t_{mp}^* u_{m,k}) d\partial\Omega - \int_{\Omega} f_j u_{jp,k}^* d\Omega. \tag{18}$$

In eqn (18),  $(\ )_k \equiv \partial(\ )/\partial x_k$ , and  $C = 1$  when  $\xi_m \in \Omega$ , and  $C = 1/2$  at a smooth part of the boundary. As compared to eqn (12) wherein the kernel  $\partial t_{jp}^*/\partial \xi_k$  is involved in the boundary integral, in the presently derived eqn (18), only the kernels  $u_{jp,i}^*$  and  $t_{mp}^*$  are involved at  $\partial\Omega$ . Note that the orders of singularity in  $u_{jp,i}^*$  and  $t_{mp}^*$ , which are equal, are nevertheless smaller than that in  $\partial t_{jp}^*/\partial \xi_k$ . The singularities in the integrals in eqn (18) are in general tractable, and the integrals in eqn (18) can be evaluated by the method suggested by Guiggiani and Casalini (1987) for two-dimensional case, by Guiggiani and Gigante (1990) for three-dimensional case, or by an alternate method described in this paper. It is noted here that some regularization techniques have also been developed for the integral involving  $\partial t_{jp}^*/\partial \xi_k$  type kernels. A comprehensive review of such regularization techniques is given in Krishnasamy *et al.* (1991). Once the tractions  $t_j$  at the boundary are completely known [for example, using the displacement boundary integral equation (11)], the displacement gradients  $u_{i,j}$  can be determined from eqn (18) (which would then become an integral equation involving  $u_{p,k}$  alone) in the interior  $\Omega$  as well as at  $\partial\Omega$ . We note also that by starting out with weak-forms of the linear momentum balance relations in the form :

$$\int_{\Omega} (\sigma_{ij,i} + f_j) \bar{u}_{j,kl} d\Omega = 0, \tag{19}$$

one may obtain, for homogeneous elastic solids, an integral relation for  $u_{q,kl}$  in the form :

$$Cu_{p,kl}(\xi_m) = \int_{\partial\Omega} (-n_j E_{ijmn} u_{m,n} u_{jp,ki}^* + n_n E_{ijmn} u_{m,i} u_{jp,ki}^* + n_k u_{p,l} \delta(x_m - \xi_m) + t_j u_{jp,kl}^*) d\partial\Omega + \int_{\Omega} f_j u_{jp,kl}^* d\Omega. \tag{20}$$

Here,  $\xi_m$  is the source point and  $x_m$  is the field point. Equations of the type of eqn (20) may be useful in plate-bending analysis, wherein the second derivative of transverse displacement  $w$  corresponds to a bending moment. Integral relations for the third and higher order derivatives of  $u_i$  may similarly be derived.

### 1.2. Small strain elastoplasticity

Here, we treat the rate problem. Let  $v_i$  be the velocities of the material particle, and in the considered small strain problem,  $\dot{\epsilon}_{ij}$  be the strain-rate, and  $x_j$  the material coordinates. The rate problem is posed by :

$$\dot{\sigma}_{j,i,j} + \dot{f}_i = 0, \tag{21}$$

$$\dot{\sigma}_{ij} = \dot{\sigma}_{ji}, \tag{22}$$

$$\dot{\sigma}_{ij} = E_{ijkl}^e (\dot{\epsilon}_{kl} - \dot{\epsilon}_{kl}^p), \tag{23}$$

$$\dot{\epsilon}_{ij} = \frac{1}{2}(v_{i,j} + v_{j,i}), \tag{24}$$

$$\dot{t}_i = n_j \dot{\sigma}_{ji}. \tag{25}$$

We assume that an appropriate plasticity theory is used [see Watanabe and Atluri (1986a) for a fairly general internal variable theory for small strain plasticity theory] such that the evolution equation for  $\dot{\epsilon}_{ij}^p$  is specified in the form :

$$\dot{\epsilon}_{ij}^p = f_{ij}(\sigma'_{ij}, r_{ij}, \dots). \quad (26)$$

Assuming that the plastic flow is deviatoric, the functions  $f_{ij}$  have for their arguments : (i) the deviator of the current stress,  $\sigma'_{ij}$ ; (ii) an internal variable such as the back-stress  $r_{ij}$  in a kinematic hardening plasticity theory, etc.

The weak-forms of eqn (21) would now be written as :

$$\int_{\Omega} (\dot{\sigma}_{ij,i} + \dot{f}_j) \bar{v}_j \, d\Omega = 0, \quad (27)$$

$$\int_{\Omega} (\dot{\sigma}_{ij,i} + \dot{f}_j) \bar{v}_{j,k} \, d\Omega = 0. \quad (28)$$

Again assuming that the solid is elastically homogeneous (i.e.  $E_{ijkl}^e$  is independent of location), we write (27) and (28) as :

$$\int_{\Omega} [E_{ijmn}^e (v_{m,ni} - \dot{\epsilon}_{mn,i}^p)] \bar{v}_j \, d\Omega = 0, \quad (29)$$

$$\int_{\Omega} [E_{ijmn}^e (v_{m,ni} - \dot{\epsilon}_{mn,i}^p)] \bar{v}_{j,k} \, d\Omega = 0. \quad (30)$$

Now we take  $\bar{v}_j$  to be the fundamental solutions of the equations :

$$(E_{ijkl}^e \bar{v}_{k,i})_{,i} + \delta(x_m - \xi_m) \delta_{jp} e_p = 0. \quad (31)$$

Repeating the algebraic manipulations in eqns (15–17) which led to eqn (18), we obtain integral equations for  $v_i$  and  $v_{i,k}$  :

$$Cv_p(\xi_m) = \int_{\partial\Omega} (\dot{t}_j v_{jp}^* - v_j t_{jp}^*) \, d\partial\Omega + \int_{\Omega} (\dot{f}_j v_{j,p}^*) \, d\Omega + \int_{\Omega} (E_{ijmn}^e \dot{\epsilon}_{mn}^p v_{jp,i}^*) \, d\Omega, \quad (32)$$

$$Cv_{p,k}(\xi_m) = \int_{\partial\Omega} (n_k E_{ijmn}^e v_{m,n} v_{jp,i}^* - \dot{t}_j v_{jp,k}^* - t_{mp}^* v_{m,k}) \, d\partial\Omega - \int_{\Omega} (\dot{f}_j v_{jp,k}^*) \, d\Omega - \int_{\Omega} (E_{ijmn}^e \dot{\epsilon}_{mn}^p v_{jp,ik}^*) \, d\Omega. \quad (33)$$

It will be shown that the singularities in the kernel  $v_{jp,ik}^*$  in the domain integral in eqn (33) are tractable, when  $\xi_m \in \Omega$  or smooth  $\partial\Omega$ .

### 1.3. Finite strain elastoplasticity

Here we use an updated Lagrangian formulation. Let  $x_i$  be the spatial coordinates of a material particle in the current configuration. Let  $\dot{S}_{ij}$  be the Truesdell stress-rate (the rate of second Piola–Kirchhoff stress as referred to the current configuration); and let  $\dot{\sigma}_{ij}^J$  be the Jaumann rate of Kirchhoff stress (which is  $J$  times the Cauchy stress, where  $J$  is the ratio of volumes). It is known [see Atluri (1980)] :

$$\dot{S}_{ij} = \dot{\sigma}_{ij}^J - D_{ik} \sigma_{kj} - \sigma_{ik} D_{kj}, \quad (34)$$

where  $D_{ij}$  is the symmetric part of the velocity gradient, i.e.

$$D_{ij} = \frac{1}{2}(v_{i,j} + v_{j,i}), \tag{35}$$

wherein  $v_i$  are velocities, and  $( )_{,i} \equiv \partial( )/\partial x_i$ . The skew-symmetric part of  $v_{i,j}$  is denoted as  $W_{ij}$ , i.e.

$$W_{ij} = \frac{1}{2}(v_{i,j} - v_{j,i}). \tag{36}$$

The rate forms of the linear and angular momentum balances are [see, Atluri (1980)]:

$$(\dot{S}_{ij} + \tau_{ik}v_{j,k})_{,i} + \dot{f}_j = 0 \tag{37}$$

and

$$\dot{S}_{ij} = \dot{S}_{ji} \tag{38}$$

where, in a dynamic problem,  $\dot{f}_i$  are appropriately defined in terms of the rate of change of inertia forces and  $( )_{,j} = \partial( )/\partial x_j$ ;  $x_j$  are current coordinates of a material particle. In eqn (37),  $\tau_{ij}$  is the Cauchy stress in the current configuration. Consistent theories of combined isotropic/kinematic hardening finite strain plasticity that are capable of modeling the available test data (at finite strain) are fully discussed in Im and Atluri (1987a, 1987b). Especially, in the case of kinematic hardening plasticity at finite strains, it is desirable [see Im and Atluri (1987a), and the references cited therein] to introduce the so-called plastic spin, denoted by  $W_{ij}^p$ . As seen in Im and Atluri (1987a) a combined isotropic/kinematic hardening plasticity may be characterized by the following evolution equations:

$$D_{ij}^p = f_{ij}(\sigma'_{ij}, D_{ij}, W_{ij}^p, \dots) \tag{39}$$

$$W_{ij}^p = g_{ij}(\sigma'_{ij}, r_{ij}, \dots) \tag{40}$$

$$\dot{r}_{ij}^J = h_{ij}(D_{ij}^p, W_{ij}^p, \dots) \tag{41}$$

and

$$\dot{\sigma}_{ij}^J = k_{ij}(D_{ij}^p, W_{ij}^p, \dots). \tag{42}$$

Here,  $r_{ij}$  is the back-stress;  $\dot{r}_{ij}^J$  the Jaumann rate of the back-stress;  $D_{ij}^p$  the plastic part of the velocity strain  $D_{ij}$ ; and  $\sigma'_{ij}$  is the deviator of the Kirchhoff stress.

Integral representations for the combined isotropic/kinematic hardening plasticity theories of the above type have been discussed in Im and Atluri (1987b). It is noted here that  $r_{ij} = 0$ ;  $W_{ij}^p = 0$  in the case of isotropic hardening. The evolution equations for  $\dot{\sigma}_{ij}^J$  is given by:

$$\dot{\sigma}_{ij}^J \equiv \dot{\sigma}_{ij} - W_{ik}\sigma_{kj} + \sigma_{ik}W_{kj} = E_{ijkl}^e(D_{kl} - D_{kl}^p) - W_{ik}^p\sigma_{kj} + \sigma_{ik}W_{kj}^p. \tag{43}$$

We restrict our attention to the case of elastically-isotropic and elastically-homogeneous solids. Thus,  $E_{ijkl}^e$  is given by eqn (4), with  $\lambda$  and  $\mu$  being independent of  $x_m$ . The weak-forms of eqn (37) are written as:

$$\int_{\Omega} [(\dot{S}_{ij} + \tau_{im}v_{j,m})_{,i} + \dot{f}_j] \bar{v}_j \, d\Omega = 0, \tag{44}$$

$$\int_{\Omega} [(\dot{S}_{ij} + \tau_{im}v_{j,m})_{,i} + \dot{f}_j] \bar{v}_{j,k} \, d\Omega = 0. \tag{45}$$

The rate of tractions  $\dot{t}_j$  are defined as :

$$\dot{t}_j \equiv n_i(\dot{S}_{ij} + \tau_{im}v_{j,m}), \tag{46}$$

where  $n_i$  are components of a unit outward normal to the boundary of the solid in its current configuration. Integrating eqn (44) by parts, applying the divergence theorem twice and making use of eqn (43), we obtain :

$$\begin{aligned} & - \int_{\partial\Omega} (\dot{t}_j \bar{v}_{jl} - v_j \bar{t}_{jl}) \, d\Omega + \int_{\Omega} (E_{ijmn}^e \bar{v}_{j,i})_{,n} v_m \, d\Omega \\ & + \int_{\Omega} [E_{ijmn}^e D_{mn}^p - (W_{im} - W_{im}^p) \tau_{mj} + \tau_{im} (W_{mj} - W_{mj}^p) + v_{i,m} \tau_{mj}] \bar{v}_{j,i} \, d\Omega + \int_{\Omega} \dot{f}_j \bar{v}_j \, d\Omega = 0. \end{aligned} \tag{47}$$

Likewise integrating eqn (45) by parts, applying the divergence theorem three times, we obtain :

$$\begin{aligned} & \int_{\partial\Omega} (\dot{t}_j \bar{v}_{j,k} + \dot{t}_m v_{m,k} - n_k E_{ijmn}^e \bar{v}_{j,i}) \, d \partial\Omega - \int_{\Omega} (E_{ijmn}^e \bar{v}_{j,i})_{,n} v_{m,k} \, d\Omega \\ & + \int_{\Omega} [E_{ijmn}^e D_{mn}^p - (W_{im} - W_{im}^p) \tau_{mj} + \tau_{im} (W_{mj} - W_{mj}^p) + v_{i,m} \tau_{mj}] \bar{v}_{j,i,k} \, d\Omega + \int_{\Omega} \dot{f}_j \bar{v}_{j,k} \, d\Omega = 0. \end{aligned} \tag{48}$$

In eqns (47) and (48),  $\dot{t}_j$  is defined as in (46), while,

$$\dot{t}_m = n_n E_{ijmn}^e \bar{v}_{j,i}. \tag{49}$$

We assume  $\bar{v}_j$  to be the fundamental solution of the equation

$$[E_{ijmn}^e \bar{v}_{m,n}]_{,i} + \delta(x_m - \xi_m) \delta_{jl} e_l = 0, \tag{50}$$

wherein  $(\ )_{,i} \equiv \partial(\ )/\partial x_i$ ;  $x_i$  are the current coordinates of a material particle. Let  $v_{jp}^*$  be the solution to the displacement in an infinite linear elastic solid along the  $i$ th direction at location  $x_m$ , due to a unit load along the  $l$ th direction at the location  $\xi_m$  in the current configuration. Using eqn (50) in eqns (47) and (48), we obtain the integral representations :

$$\begin{aligned} C v_p(\xi_m) &= \int_{\partial\Omega} (\dot{t}_j v_{jp}^* - v_j \dot{t}_{jp}^*) \, d \partial\Omega \\ &+ \int_{\Omega} [E_{ijmn}^e D_{mn}^p - (W_{im} - W_{im}^p) \tau_{mj} + \tau_{im} (W_{mj} - W_{mj}^p) + v_{i,m} \tau_{mj}] v_{jp,i}^* \, d\Omega + \int_{\Omega} \dot{f}_j v_{jp}^* \, d\Omega \end{aligned} \tag{51}$$

and,

$$\begin{aligned} C v_{p,k}(\xi_m) &= \int_{\partial\Omega} (n_k E_{ijmn}^{(e)} v_{m,n} v_{jp,i}^* - \dot{t}_j v_{jp,k}^* - \dot{t}_{mp}^* v_{m,k}) \, d \partial\Omega \\ &- \int_{\Omega} [E_{ijmn}^e D_{mn}^p - (W_{im} - W_{im}^p) \tau_{mj} + \tau_{im} (W_{mj} - W_{mj}^p) + v_{i,m} \tau_{mj}] v_{jp,ik}^* \, d\Omega - \int_{\Omega} \dot{f}_j v_{jp,k}^* \, d\Omega, \end{aligned} \tag{52}$$

where  $(\ )_{,k}$  in eqn (52) denotes  $\partial(\ )/\partial x_k$ ,  $x_k$  the current coordinates of a material particle, and  $C = 1$  in  $\Omega$ , and  $C = 1/2$  at a smooth boundary. The kernels  $v_{jp,i}^*$  and  $\dot{t}_{mp}^*$  have the same order of singularity, and these singularities are tractable in the boundary integral, as  $\xi_m$  tends to the boundary. The singularities in the kernel  $v_{jp,ik}^*$  in the domain integral are also tractable, when  $\xi_m$  lies inside  $\Omega$  or at smooth  $\partial\Omega$ . Further insight will be provided in this

article, on the implementation of eqn (52). On the other hand,  $i_i$  at  $\partial\Omega$  may be solved from the usual integral representation for  $v_p$  (51). Once  $i_i$  at  $\partial\Omega$  are solved for, eqn (52) may be viewed as an integral equation for  $v_{p,k}$  alone. From a numerical view point, it is clear that the integral equation for  $v_p$  alone involves velocity gradients as unknowns in the domain. Thus, an iterative algorithm is imperative for the complete evaluation of velocities and velocity gradients inside  $\Omega$  as well as at  $\partial\Omega$ .

1.4. Geometrically non-linear behavior of a semi-linear solid

We use a total Lagrangian description of motion [see Atluri (1980)] for details. Let  $X_A$  and  $x_i$ , respectively, be the coordinates of a material particle, before and after the finite deformation of the solid, in a fixed Cartesian frame. Let the second Piola–Kirchhoff stress tensor, and the Green–Lagrange strain tensor, referred to the undeformed configuration, be  $S_{AB}$  and  $g_{CD}$ , respectively. We consider the material to be semi-linear and isotropic, such that :

$$S_{AB} = E_{ABCD}g_{CD}, \tag{53}$$

and

$$E_{ABCD} = \lambda\delta_{AB}\delta_{CD} + \mu(\delta_{AC}\delta_{BD} + \delta_{AD}\delta_{BC}). \tag{54}$$

Let  $u_A$  be the displacements of a material particle, such that :

$$x_A = X_A + u_A, \tag{55}$$

whereupon,

$$g_{AB} = \frac{1}{2}(u_{A,B} + u_{B,A} + u_{i,A}u_{i,B}), \tag{56}$$

where  $( )_{,A} \equiv \partial( )/\partial X_A$ . Use of eqn (56) in eqn (53) leads to :

$$S_{AB} = E_{ABCD}u_{C,D} + \frac{1}{2}E_{ABCD}u_{m,C}u_{m,D}. \tag{57}$$

The equations of linear and angular momentum balance are :

$$(S_{AB}F_{iB})_{,A} + f_i = 0 \tag{58}$$

and

$$S_{AB} = S_{BA}, \tag{59}$$

where  $F_{iB} \equiv \partial x_i/\partial X_B$  and  $f_i$  are body forces per unit initial volume. The traction components in the deformed solid are represented as :

$$t_i = n_A S_{AB} F_{iB}, \tag{60}$$

where  $n_A$  are the components of a unit outward normal to the boundary in the initial configuration. Note that  $t_i$  are measured per unit area at the boundary of the undeformed solid. Let  $\Omega$  and  $\Omega_o$  refer to the final and initial configurations of the solid.

If the weak-forms of eqn (58) are written as :

$$\int_{\Omega_o} \{ (S_{AB}F_{iB})_{,A} + f_i \} \bar{u}_i \, d\Omega_o = 0, \tag{61}$$

then integrating eqn (61) by parts, applying the divergence theorem, and choosing the test functions  $\bar{u}_i$  to be the fundamental solutions of the following equations :

$$\delta_{iB}(E_{ABCD}\bar{u}_{C,D})_{,A} + \delta_{iL}\delta(X_M - \xi_M)e_L = 0, \tag{62}$$



i.e. choosing  $\bar{u}_i$  to be the fundamental solutions to the Navier equations of linear elasticity written in the coordinates of the undeformed solid, one can deduce from (55) that :

$$Cu_P = \int_{\partial\Omega_o} (t_i u_{iP}^* - t_{kP}^* u_k) \, d\partial\Omega_o - \int_{\Omega_o} \frac{1}{2} E_{ABCD} u_{m,C} u_{m,D} u_{BP,A}^* \, d\Omega_o - \int_{\Omega_o} S_{AB} u_{i,B} u_{iP,A}^* \, d\Omega_o + \int_{\Omega_o} f_i u_{iP}^* \, d\Omega_o, \quad (63)$$

where  $C = 1$  in  $\Omega_o$  and  $C = 1/2$  at a smooth  $\partial\Omega_o$ . In eqn (63)  $(\ )_{,L} \equiv \partial(\ )/\partial X_L$ . The quantities  $u_k$  and  $t_i$  are assumed to be specified over a part of  $\partial\Omega_o$ , and are direct unknowns over the remainder of  $\partial\Omega_o$ . Equations of the type of (63) were used in O'Donoghue and Atluri (1987) and Zhang and Atluri (1986) in solving problems posed by the Von Karman type non-linear theories of plates and shallow shells, by integral methods. Instead of (61), the weak-forms of eqn (58) may be written as :

$$\int_{\Omega_o} \{ (S_{AB} F_{iB})_{,A} + f_i \} \bar{u}_{i,D} \, d\Omega_o = 0, \quad (64)$$

where  $(\ )_{,D} = \partial(\ )/\partial X_D$ . Integrating (58) by parts, applying the divergence theorem thrice, and making use of eqns (57) and (60), we have :

$$\int_{\partial\Omega_o} (t_i \bar{u}_{i,D} + \bar{t}_M u_{M,D} - n_D E_{ABMN} u_{M,N} \bar{u}_{B,A}) \, d\partial\Omega_o - \int_{\Omega_o} (E_{ABMN} \bar{u}_{B,A})_{N} u_{M,D} \, d\Omega_o - \int_{\Omega_o} \frac{1}{2} E_{ABMN} u_{k,M} u_{k,N} \bar{u}_{B,AD} \, d\Omega_o - \int_{\Omega_o} S_{AB} u_{i,B} \bar{u}_{i,AD} \, d\Omega_o + \int_{\Omega_o} f_i \bar{u}_{i,D} \, d\Omega_o = 0. \quad (65)$$

In eqn (65),  $(\ )_{,D} \equiv \partial(\ )/\partial X_D$  and  $\bar{t}_M$  are tractions of a pseudo-linear solid :

$$\bar{t}_M = n_N E_{ABMN} \bar{u}_{B,A}. \quad (66)$$

If  $\bar{u}_B$  in eqn (65) is taken to the fundamental solution as in eqn (62), we may write :

$$\bar{u}_{B,A} = u_{BL,A}^* e_L, \quad (67)$$

$$\bar{t}_M = t_{ML}^* e_L \quad (68)$$

and

$$\bar{u}_{i,AD} = u_{iL,AD}^* e_L. \quad (69)$$

Using eqns (67–69) in eqn (65), one obtains :

$$Cu_{P,D} = \int_{\partial\Omega_o} (n_D E_{ABMN} u_{M,N} u_{BP,A}^* - t_i u_{iP,D}^* - t_{MP}^* u_{MD}) \, d\partial\Omega_o + \int_{\Omega_o} (\frac{1}{2}) E_{ABMN} u_{k,M} u_{k,N} u_{BP,AD}^* \, d\Omega_o + \int_{\Omega_o} S_{AB} u_{i,B} u_{iP,AD}^* \, d\Omega_o - \int_{\Omega_o} f_i u_{iP,D}^* \, d\Omega_o. \quad (70)$$

Here  $C = 1$  in  $\Omega_o$ , and  $C = 1/2$  at a smooth  $\partial\Omega$ ; and  $(\ )_{,A} \equiv (\ )/\partial X_A$ . The tractions  $t_i$  are presumed to be given over a part of  $\partial\Omega_o$  and are direct unknowns over the remainder of  $\partial\Omega_o$ .

At the boundary  $\partial\Omega_o$ , eqn (70) involves the kernels  $u_{BP,A}^*$  and  $t_{MP}^*$  which have the same order of singularity, and are quite tractable numerically. Likewise, the domain integrals involve the singular kernels  $u_{BP,AD}^*$ , which again, are tractable numerically. Alternatively,

eqns (63) and (70) may together be used, iteratively, to determine  $u_p$  and  $u_{p,D}$  at  $\partial\Omega_o$  as well as in  $\Omega_o$ . Thus, for instance, the unknown  $t_i$  at  $\partial\Omega_o$  are presumed to be solved from eqn (63), and when these are used in eqn (70), it would then become an integral equation for  $u_{p,D}$ .

1.5. Evaluation of free terms in the integral representation of velocity gradients

We consider the case of a finitely deformed elastic-plastic solid undergoing isotropic hardening (i.e.  $W_{ij}^p = 0$ ) as a generic case. The following arguments apply equally well for two- and three-dimensional problems.

First consider the case when the source point  $\xi$  is inside  $\Omega$ , in the current configuration of the finitely deformed solid, when an updated Lagrangian approach is used. Integrating eqn (45) by parts, and applying the divergence theorem once to the region free from singularities, i.e.  $\Omega - \varepsilon$  in Fig. 1, we have :

$$\int_{\partial\Omega} i_j \bar{v}_{j,k} \, d\partial\Omega - \int_{\Omega-\varepsilon} E_{ijmn}^c v_{m,n} \bar{v}_{j,ik} \, d\Omega - \int_{\Omega-\varepsilon} (-E_{ijmn}^c D_{mn}^p + W_{im} \tau_{mj} - W_{mj} \tau_{im} - v_{i,m} \tau_{mj}) \bar{v}_{j,ik} \, d\Omega + \int_{\Omega-\varepsilon} f_j \bar{v}_{j,k} \, d\Omega + \int_{\partial\varepsilon} n_i (\dot{S}_{ij} + \tau_{im} v_{j,m}) \bar{v}_{j,k} \, d\partial\varepsilon + \int_{\varepsilon} f_j \bar{v}_{j,k} \, d\Omega + \int_{\varepsilon} [\dot{S}_{ij} + \tau_{im} v_{j,m}]_i \bar{v}_{j,k} \, d\Omega = 0, \tag{71}$$

where  $i_j$  is defined in eqn (46), and  $( )_{,k} = \partial( )/\partial x_k$ . Integrating (71) by parts, and applying the divergence theorem two more times, and considering that  $\bar{v}_m$  are fundamental solutions to eqn (50), one obtains :

$$\int_{\varepsilon\Omega} (i_j v_{jp,k}^* + t_{mp}^* v_{m,k} - n_k E_{ijmn}^c v_{m,n} v_{jp,i}^*) \, d\partial\Omega + \int_{\Omega} (E_{ijmn}^c D_{mn}^p - W_{im} \tau_{mj} + \tau_{im} W_{mj} + v_{i,m} \tau_{mj}) v_{jp,ik}^* \, d\Omega + \int_{\Omega} f_j v_{jp,k}^* \, d\Omega + \varepsilon \xrightarrow{Lt} 0 \left\{ \int_{\partial\varepsilon} t_{mp}^* v_{m,k} \, d\partial\varepsilon - \int_{\partial\varepsilon} n_i^c (E_{ijmn}^c D_{mn}^p - W_{im} \tau_{mj} + \tau_{im} W_{mj} + v_{i,m} \tau_{mj}) v_{jp,k}^* \, d\partial\varepsilon + \int_{\varepsilon} f_j v_{jp,k}^* \, d\varepsilon + \int_{\varepsilon} (\dot{S}_{ij} + \tau_{im} v_{j,m})_i v_{jp,k}^* \, d\varepsilon \right\} = 0. \tag{72}$$

We now consider the limiting terms in eqn (72), one by one. First,

$$\varepsilon \xrightarrow{Lt} 0 \int_{\varepsilon} (\dot{S}_{ij} + \tau_{im} v_{j,m})_i v_{jp,k}^* \, d\varepsilon = [(\dot{S}_{ij} + \tau_{im} v_{j,m})_i]_P \varepsilon \xrightarrow{Lt} 0 \int_{\varepsilon} v_{jp,k}^* \, d\varepsilon, \tag{73}$$

where  $P$  is the source point  $\xi$  in  $\Omega$ . Due to the inherent property of  $v_{jp,k}^*$  kernel in the Kelvin's solution, it can be seen that :

$$\varepsilon \xrightarrow{Lt} 0 \int_{\varepsilon} v_{jp,k}^* \, d\varepsilon = 0. \tag{74}$$

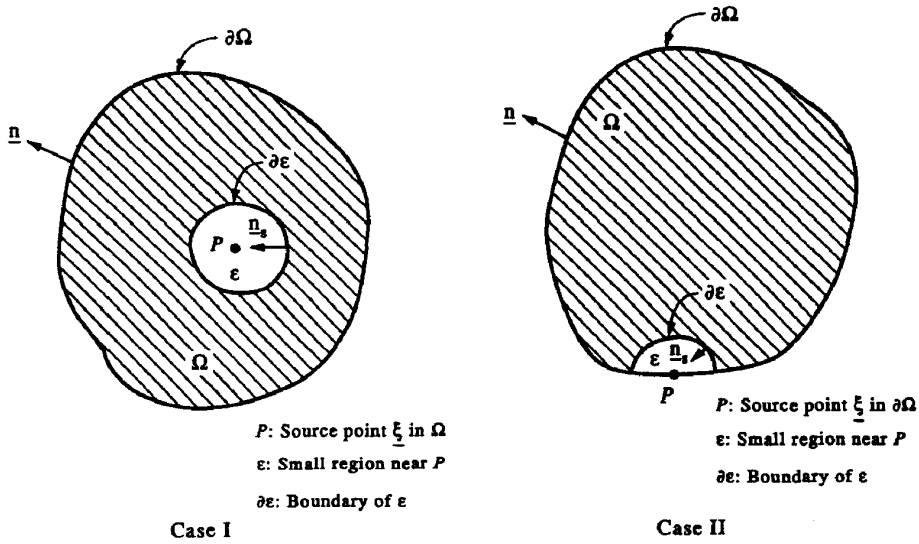


Fig. 1. Evaluation of singular integrals in a sense of Cauchy principal value.

Similarly, it is seen that :

$$\epsilon \xrightarrow{Lt} 0 \int_{\epsilon} \dot{f}_j v_{jp,k}^* d\epsilon = 0. \tag{75}$$

We now consider the limiting term :

$$\begin{aligned} \epsilon \xrightarrow{Lt} 0 \int_{\partial\epsilon} [t_{mp}^* v_{m,k} - n_i^e (E_{ijmn}^e D_{mn}^p - W_{im} \tau_{mj} + \tau_{im} W_{mj} + v_{i,m} \tau_{mj}) v_{jp,k}^*] d \partial\epsilon = v_{p,k} \\ - [E_{ijmn}^e D_{mn}^p - W_{im} \tau_{mj} + \tau_{im} W_{mj} + v_{i,m} \tau_{mj}]_P \epsilon \xrightarrow{Lt} 0 \int_{\partial\epsilon} n_i^e v_{jp,k}^* d \partial\epsilon. \end{aligned} \tag{76}$$

It can be shown that :

$$\begin{aligned} \epsilon \xrightarrow{Lt} 0 \int_{\partial\epsilon} n_i^e v_{jp,k}^* d \partial\epsilon &= \frac{-1}{16(1-\nu)G} \{ \delta_{ip} \delta_{kj} + \delta_{ij} \delta_{kp} - (7-8\nu) \delta_{ik} \delta_{pj} \} \\ &\text{for two-dimensional plane strain} \\ &= \frac{-1}{30(1-\nu)G} \{ \delta_{ip} \delta_{kj} + \delta_{ij} \delta_{kp} - (9-30\nu) \delta_{ik} \delta_{pj} \} \\ &\text{for three-dimensional problem,} \end{aligned} \tag{77}$$

where  $G$  is the shear modulus. Hence, the integral representation for  $v_{p,k}$  ( $\equiv \partial v_p / \partial x_k$ ) at the source point  $P$  ( $= \underline{\xi}$ ) inside  $\Omega$  can be written, using (74), (75), (76) and (77) in eqn (72), as :

$$\begin{aligned} C v_{p,k}(\underline{\xi}) &= \int_{\partial\Omega} (n_k E_{ijmn}^e v_{m,n} v_{jp,i}^* - \dot{t}_j v_{jp,k}^* - t_{mp}^* v_{m,k}) d \partial\Omega \\ &\quad - \int_{\Omega} (E_{ijmn}^e D_{mn}^p - W_{im} \tau_{mj} + \tau_{im} W_{mj} + v_{i,m} \tau_{mj}) v_{jp,ik}^* d\Omega \\ &\quad - \int_{\Omega} \dot{f}_j v_{jp,k} d\Omega + [E_{ijmn}^e D_{mn}^p - W_{im} \tau_{mj} + \tau_{im} W_{mj} + v_{i,m} \tau_{mj}]_P F_{ijpk}, \end{aligned} \tag{78}$$

where  $[ ]_P$  refers to the quantity  $[ ]$  evaluated at the source point  $P (= \xi)$  in  $\Omega$ , and  $F_{ijpk}$  refers to the free terms given in eqn (77), and  $C = 1$ .

When the source point  $P (= \xi)$  is taken in the limit to a smooth  $\partial\Omega$ , a similar analysis as described in eqns (72)–(77) may be carried out. The resulting expression for  $v_{p,k}$  at  $\xi \in$  smooth  $\partial\Omega$  will be similar to that in eqn (78), except that  $C = (1/2)$ ; and  $F_{ijpk}$  should be replaced by  $(F_{ijpk}/2)$ .

1.6. Numerical analysis: small and finite strain elastoplasticity using the nonhyper-singular integral equations for velocity gradients

The analyses of small and finite strain elastoplasticity are presented, along with the detailed numerical implementations for the numerical evaluations of singular integrals. The numerical implementations have been discussed in Lachat and Watson (1976), and Banerjee and Raveendra (1986). An elastoplastic constitutive equation, that is employed in the present analysis, is described. The methods of updating the stresses in the finite strain elastoplastic analysis, using an objective stress integration scheme and the mid-point radial return algorithm, are presented. The numerical results demonstrate that the use of the nonhyper-singular integral equation leads to a superior numerical accuracy.

1.6.1. Elastic-plastic constitutive equation. Here, we consider a general type of elastic-plastic constitutive model, which includes the isotropic, the kinematic and the combined isotropic/kinematic hardening behavior of the solid at large strains. It has been pointed out by several authors [see Atluri (1984), Lee *et al.* (1983), Reed and Atluri (1985)] that in a kinematic hardening large strain plasticity model, if the evolution equations for the Jaumann rates of the Kirchhoff stress and of the back-stress, respectively, are simply taken to be linear functions of the plastic component of the velocity strain, certain anomalous consequences, such as an oscillatory stress response of the material in finite simple shear, may result. More general evolution equations, especially to account for the noncoaxiality of the Cauchy stress and the Cauchy-like back-stress in shear and nonproportional loadings, have been attempted by Atluri (1984) and by Reed and Atluri (1983) to suppress the above physically unacceptable oscillatory stress responses. Although these methods based on formal continuum mechanics were quite successful for the simple shear case, the physics and micromechanics of finite plastic flow indicate that a more consistent large strain elastoplastic constitutive law should involve an evolution equation for the plastic component of the spin tensor. Such an elastic-plastic constitutive model has been developed, for instance, in Im and Atluri (1987a,b), which is the finite strain version of the endochronic constitutive model of Watanabe and Atluri (1986a,b). Here, the concept of a material director triad is introduced and the relaxed intermediate configuration is chosen to be isoclinic. The plastic spin tensor is defined through internal time. Such an endochronic constitutive model (for large strain elastoplasticity) employed here, can be summarized as follows.

Let  $N_{ij}$  be the normal to the yield surface in the deviatoric Kirchhoff stress space. When the stress is on the yield surface and  $N_{ij}D_{ij} \geq 0$ , the process is a plastic process.

$$N_{ij} = (\tau'_{ij} - r_{ij}) / \|\tau'_{kl} - \tau_{kl}\|, \tag{79}$$

$$\zeta = D_{ij}N_{ij}/C, \tag{80}$$

$$D_{ij}^p = N_{ij}\zeta, \tag{81}$$

$$W_{ij}^p = \Omega_{ij}\zeta, \tag{82}$$

$$\Omega_{ij} = \left\{ \frac{m_1(r_{ik}\tau'_{kj} - \tau'_{ik}r_{kj})}{\tau_y^2 f^2(\zeta)} + \frac{m_2(r_{ik}r_{kl}\tau'_{lj} - \tau'_{ik}r_{kl}r_{lj})}{\tau_y^3 f^3(\zeta)}, \frac{m_3(r_{ik}\tau'_{kl}\tau'_{lj} - \tau'_{ik}\tau'_{kl}r_{lj})}{\tau_y^3 f^3(\zeta)} \right\}, \tag{83}$$

$$(\tau'_{ij} - r_{ij})(\tau'_{ij} - r_{ij}) = \tau_y f^2(\zeta), \tag{84}$$

$$\dot{\tau}_{ij}^j = \lambda(D_{kk})\delta_{ij} + 2\mu(D_{ij} - D_{ij}^p) - W_{ik}^p \tau_{kj} + \tau_{ik} W_{kj}^p, \quad (85)$$

$$\dot{r}_{ij}^j = 2\mu\rho_1 D_{ij}^p - \frac{\alpha r_{ij}(D_{kl}^p D_{kl}^p)^{1/2}}{f(\zeta)} - W_{ik}^p r_{kj} + r_{ik} W_{kj}^p, \quad (86)$$

where,  $r_{ij}$  is the back-stress and  $\tau_{ij}^j$  is the deviatoric part of Kirchhoff stress  $\tau_{ij}$ .  $f(\zeta)$  and  $r_{ij}$  represent the expansion and translation of von Mises type yield surface.  $D_{ij}^p$  and  $W_{ij}^p$  are the rate of plastic strain and the plastic spin, respectively.  $\zeta$  represents the internal time variable. It is seen that  $\Omega_{ij}$  accounts for the noncoaxiality of the tensors  $\tau_{ij}^j$  and  $r_{ij}$ . The reader is referred to Im and Atluri (1986a,b) for further details of the constitutive model.

1.6.2. *The BEM formulation.* As described earlier, the integral representation for the velocity in the case of finite strain elastoplasticity can be written as,

$$C_{pq}v_q(\xi_m) = \int_{\partial\Omega} (\dot{t}_j v_{jp}^* - v_j \dot{t}_{jp}^*) d\partial\Omega + \int_{\Omega} \{E_{ijmn}^e D_{mn}^p - (W_{im} - W_{im}^p)\tau_{mj} + \tau_{im}(W_{mj} - W_{mj}^p) + v_{i,m}\tau_{mj}\} v_{jp,i}^* d\Omega + \int_{\Omega} \dot{f}_j v_{jp}^* d\Omega. \quad (87)$$

Here  $C_{ij} = \delta_{ij}$  in the interior and  $\frac{1}{2}\delta_{ij}$  at a smooth boundary point. The above equation, when discretized and applied at the boundary, results in the standard boundary element system of equations:

$$\mathbf{H}\mathbf{v} = \mathbf{G}\dot{\mathbf{t}} + \mathbf{Q}\mathbf{g}, \quad (88)$$

where  $\mathbf{v}$ ,  $\dot{\mathbf{t}}$  and  $\mathbf{g}$  are the velocities and the traction rates at the boundary, and the velocity gradients in the interior, respectively; and  $\mathbf{H}$ ,  $\mathbf{G}$  and  $\mathbf{Q}$  are the associated matrices.

The standard BEM formulation makes use of eqn (87), and obtains the strain field by differentiating it with respect to the load point  $\xi_j$ . Thus,

$$v_{p,k}(\xi_m) = \int_{\partial\Omega} \left[ \frac{\partial v_{jp}^*(x_m, \xi_m)}{\partial \xi_k} \dot{t}_j(x_m) - \frac{\partial \dot{t}_{jp}^*(x_m, \xi_m)}{\partial \xi_k} v_j(x_m) \right] d(\partial\Omega) + \int_{\Omega} \{E_{ijmn}^e D_{mn}^p - (W_{im} - W_{im}^p)\tau_{mj} + \tau_{im}(W_{mj} - W_{mj}^p) + v_{i,m}\tau_{mj}\} \frac{\partial v_{jp,i}^*}{\partial \xi_k} d\Omega + [E_{ijmn}^e D_{mn}^p - W_{im}\tau_{mj} + \tau_{im}W_{mj} + v_{i,m}\tau_{mj}]_p F_{ijpk} + \int_{\Omega} \dot{f}_j \frac{\partial v_{jp}^*}{\partial \xi_k} d\Omega. \quad (89)$$

$F_{ijkl}$  is defined as shown in eqns (77) and (78).

This method gives rise to  $\partial \dot{t}_{jp}^* / \xi_k$  type kernels, which are hyper-singular, when  $\xi_m$  tends to a boundary point. Hence, this predicament gives rise to a two tier system of evaluation for the stress field.

The following direct integral equation (in the absence of body forces) for the velocity gradients has been obtained earlier in this paper.

$$Cv_{p,k}(\xi_m) = \int_{\partial\Omega} (n_k E_{ijmn}^{(e)} v_{m,n} v_{jp,i}^* - \dot{t}_j v_{jp,k}^* - \dot{t}_{mp}^* v_{m,k}) d\partial\Omega - \int_{\Omega} \{E_{ijmn}^e D_{mn}^p - (W_{im} - W_{im}^p)\tau_{mj} + \tau_{im}(W_{mj} - W_{mj}^p) + v_{i,m}\tau_{mj}\} v_{jp,ik}^* d\Omega + [E_{ijmn}^e D_{mn}^p - W_{im}\tau_{mj} + \tau_{im}W_{mj} + v_{i,m}\tau_{mj}]_p F_{ijpk} - \int_{\Omega} \dot{f}_j v_{jp,k}^* d\Omega. \quad (90)$$

Here,  $C = 1$  in the interior and  $\frac{1}{2}$  at a smooth boundary point. The kernels  $u_{j,p,k}^*$  and  $t_{ip}^*$  have the same order of singularity and in general are tractable from a numerical point of view. Note also that as  $x_m$  tends to  $\partial\Omega$ , the singularities in the new representation, eqn (90) are of lower order as compared to those in eqn (89). Equation (90), when discretized and applied at the boundary, results in the following system of equations:

$$\mathbf{H}_d \mathbf{v}_d = \mathbf{G}_d \dot{\mathbf{t}} + \mathbf{Q}_d \mathbf{g} \tag{91}$$

where  $\mathbf{v}_d, \dot{\mathbf{t}}$  are, respectively, the velocity gradients and tractions at the boundary,  $\mathbf{g}$  is the velocity gradient in the interior and  $\mathbf{H}_d, \mathbf{G}_d$  and  $\mathbf{Q}_d$  are the associated matrices. It is interesting to note that the order of singularity in  $\mathbf{H}_d$  and  $\mathbf{G}_d$  terms is the same as that of the terms in  $\mathbf{H}$  in eqn (88).

The unknown boundary velocities and traction rates could be obtained from eqn (88) as in the standard BEM approach. Once the complete velocities and traction rate field are completely ascertained on the boundary, eqn (91) could be used to solve for the boundary velocity gradients. Finally, the velocity gradients could be evaluated pointwise, in the interior, [using eqn (90)], once the velocity gradients at the boundary are known. Hence the stress field could be determined by the elastoplastic constitutive equation in a uniform manner. The velocity gradients in the standard formulation are obtained by direct differentiation of the velocity integral equation (89). The resulting equation gives rise to hyper-singularities as the source point is taken to the boundary. Hence the velocity gradients on the boundary are obtained by numerically differentiating the velocities at the boundary. An initial strain type iterative method is employed in the calculation of elastoplasticity. As for the present method the integral equation for the velocity gradients does not involve hyper-singularities [eqn (90)] and hence is applicable when the source point is in the interior as well as on the boundary.

Once the  $D_{ij}$  is computed, the objective stress-rate  $\dot{\tau}'_{ij}$  is computed using a generalized mid-point algorithm and an objective time integration scheme. The details of both algorithms are described in Im and Atluri (1987b), Atluri (1985), Rubinstein and Atluri (1983), and Reed and Atluri (1983). The computational algorithms are briefly described here. These algorithms are quite effective to obtain an accurate solution in computational elastic-plastic analysis especially for the finite strain case.

The mid-point radial return algorithm for determining  $\dot{\tau}'_{ij}$  (Jaumann rate of Kirchhoff stress) from  $D_{ij}$  (rate of strain) is summarized as follows,

1. Compute  $D_{ij}$ .
2. Check if

$$\{(\tau'_{ij} + 2\mu D_{ij} \Delta t)(\tau'_{ij} + 2\mu D_{ij} \Delta t)\} \begin{matrix} \geq \\ \leq \end{matrix} R_N^2, \tag{92}$$

where  $R_N$  is the current radius of the yield cylinder, and  $\Delta t$  is the time increment. If  $\geq R_N^2$ , then the process is plastic. Go to step 3.

3. Define a generalized mid-point normal to the yield solution

$$N_{\theta ij} = \frac{(\tau'_{ij} + 2\mu\theta D_{ij} \Delta t) - r_{ij}}{\|(\tau'_{kl} + 2\mu\theta D_{kl} \Delta t) - r_{kl}\|}, \tag{93}$$

where,  $0 \leq \theta \leq 1$  and  $\theta \Delta t$  shows a time point in the current time step ( $t_N \rightarrow t_N + \Delta t$ ).

4. Define

$$\xi = \frac{1}{C_\theta} (N_{\theta ij} D_{ij}).$$

5. Compute the Jaumann stress rate

$$\dot{\tau}'_{ij} = 2\mu \left[ D_{ij} - \frac{1}{C_\theta} N_{\theta mn} D_{mn} N_{\theta ij} \right] - (\Omega_{im} \tau_{mj} - \tau_{im} \Omega_{mj}) \frac{N_{\theta kl} D_{kl}}{C_\theta} \tag{94}$$

and

$$\dot{\tau}'_{kk} = (2\mu + 3\lambda)D_{kk}.$$

#### 6. Compute the rate of back-stress

$$\dot{\tau}'_{ij} = 2\mu \frac{\rho_1}{C_\theta} (N_{\theta kl} D_{kl}) N_{\theta ij} - \alpha r_{ij} \frac{N_{\theta kl} D_{kl}}{C_\theta} - (\Omega_{ik} r_{kj} - r_{ik} \Omega_{kj}) \frac{N_{\theta mn} D_{mn}}{C_\theta}. \quad (95)$$

The objective stress integration scheme, for the finite strain case, to determine the material stress increment from the Jaumann stress-rate evaluated through the mid-point radial return algorithm is summarized as follows. Let  $Q_{ij}(t)$  be the rotation of the material particle with respect to the reference time  $t_N$ , which is the beginning of the current time step. The Kirchhoff stress  $\tau_{ij}$  at the time  $t_N + \Delta t$  can be given by the objective stress integral,

$$\begin{aligned} \tau_{ij}(t_N + \Delta t) &= J^{-1}(t_N + \Delta t) Q_{ki}(t_N + \Delta t) \tau_{ki}(t_N) Q_{lj}(t_N + \Delta t) \\ &\quad + \int_t^{t+\Delta t} J^{-1}(\xi) \cdot Q_{ki}(t + \Delta t) Q_{km}(\xi) \dot{\sigma}'_{mn}(\xi) Q_{ln}(\xi) Q_{lj}(t_N + \Delta t) d\xi, \end{aligned} \quad (96)$$

where,  $\dot{\sigma}'_{mn}$  is the Jaumann rate of Cauchy stress. The above expression is approximated for the finite time step  $t_N \rightarrow t_N + \Delta t$  as,

$$\begin{aligned} \tau_{ij}(t_N + \Delta t) &= J^{-1}(t_N + \Delta t) Q_{ki}(t_N + \Delta t) \tau_{ki}(t_N) Q_{lj}(t_N + \Delta t) \\ &\quad + J^{-1}(t_N + \frac{1}{2}\Delta t) Q_{ki}(t_N + \Delta t) Q_{km}(t_N + \frac{1}{2}\Delta t) \dot{\sigma}'_{mn}(t_N + \frac{1}{2}\Delta t) Q_{ln}(t_N + \frac{1}{2}\Delta t) Q_{lj}(t_N + \Delta t) \Delta t. \end{aligned} \quad (97)$$

Here,  $Q_{ij}(t_N + \theta\Delta t)$  ( $0 \leq \theta \leq 1$ ) is derived by,

$$Q_{ij}(t_N + \theta\Delta t) = \delta_{ij} + \frac{\sin(\omega\theta\Delta t)}{\omega} W_{ij} + \frac{\{1 - \cos(\omega\theta\Delta t)\}}{\omega^2} W_{ik} W_{kj}, \quad (98)$$

where,

$$\omega = \frac{1}{2} W_{ij} W_{ij}.$$

**1.6.3. Regularization of boundary integrals.** As seen from eqn (90), the boundary integrals in the velocity gradient expression involve Cauchy principal value integrals. Hence proper care needs to be exercised in evaluating these. As in Fig. 2,  $BOC$  is the boundary segment where the source point  $O$  lies and let  $P$  be the field point. The straight line  $EOD$  is a tangent to the curve  $BOC$  at  $O$  and let  $EC$  and  $BD$  be perpendiculars to the line  $EOD$ . The points  $B$  and  $C$  are the ends of the segment under consideration. Let  $r$  be the distance between the source point  $O$  and field point  $P$ . For illustrative purposes, let us consider the integral:

$$I_1 = \int_{\partial\Omega} \dot{t}_j(x_m) v_{jp,k}^*(x_m, \xi_m) d(\partial\Omega). \quad (99)$$

When the traction components  $t_j$  are expressed as nodal tractions multiplied by the associated shape functions, the resulting singular integral to come out of  $I_1$  would take the following generic form:

$$I_2 = \int_{\partial\Omega} N_o \dot{t}_j(x_m^o) v_{jp,k}^*(x_m, \xi_m) d(\partial\Omega). \quad (100)$$

Here  $N_o$  is the shape function associated with point  $O$ , and  $t_j(x_m^o)$  corresponds to the nodal

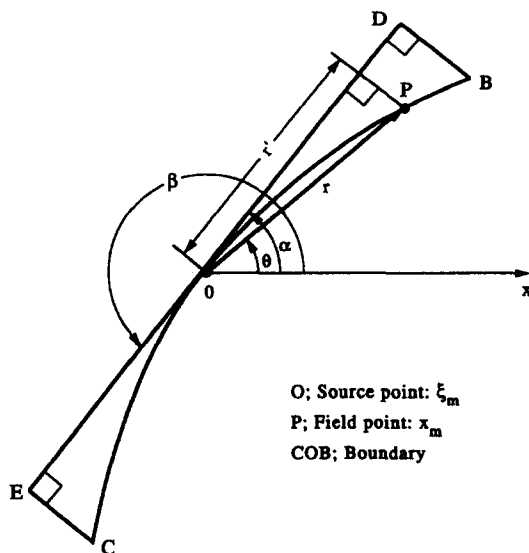


Fig. 2. Numerical implementation of singular boundary integrals.

traction at the source point, i.e. point  $O$ . The singular integral  $I_2$  can also be written in the following form

$$\begin{aligned}
 I_2 &= i_j(x_m^o) \int_{\partial\Omega} (N_o - 1) v_{jp,k}^*(x_m, \xi_m) d(\partial\Omega) + i_j(x_m^o) \int_{\partial\Omega} v_{jp,k}^*(x_m, \xi_m) d(\partial\Omega) \\
 &= I_3 + t_j(x_m^o) I_4.
 \end{aligned}
 \tag{101}$$

For simplicity, the shape function  $N_o$  can be taken to be linear. The integral  $I_3$  in the above equation is regular and hence tractable from a numerical point of view. From here onwards, we will consider only the integral  $I_4$  which appears to be singular. As per Fig. 2, the integral  $I_4$  would take the following form

$$I_4 = \int_{BOC} v_{jp,k}^* dS.
 \tag{102}$$

Due to the inherent property of the  $v_{jp,k}^*$  kernel, it could be expressed (for two-dimensional problems) in the following form

$$v_{jp,k}^* = \frac{f(\theta)}{r}, \quad f(\theta) = -f(\theta + \pi).
 \tag{103}$$

Here,  $r$  is the distance between the source point and the field point.  $\theta$  is the angle made by the line connecting the source point and field point with the  $x$ -axis. Substituting the expression for  $v_{jp,k}^*$  in eqn (103) into eqn (102) we have

$$\begin{aligned}
 I_4 &= \int_{BOC} \frac{f(\theta)}{r} dS = \int_{BO} \left\{ \frac{f(\theta)}{r} - \frac{f(\alpha)}{r'} \left| \frac{ds'}{ds} \right| \right\} ds \\
 &\quad + \int_{OC} \left\{ \frac{f(\theta)}{r} - \frac{f(\beta)}{r'} \left| \frac{ds'}{ds} \right| \right\} ds + \int_{DO} \frac{f(\alpha)}{r} dS' + \int_{OE} \frac{f(\beta)}{r} dS'.
 \end{aligned}
 \tag{104}$$

Note here, that the angles  $\alpha$  and  $\beta$  are constants and  $\theta$  varies as the field point moves along the arc (Fig. 2). The integrals along  $BO$  and  $OC$  in eqn (104) are regular and hence are



numerically tractable. Let us define the sum of the integrals over the straight lines  $DO$  and  $OE$  as in  $I_5$ . Thus

$$I_5 = \int_{DO} \frac{f(\alpha)}{r} dS' + \int_{OE} \frac{f(\beta)}{r} dS'. \tag{105}$$

Evaluating  $I_5$  in the sense of Cauchy principal values, we have

$$\begin{aligned} I_5 &= \lim_{\varepsilon \rightarrow 0} \{ [-\ln |r| f(\alpha)]_D^{-\varepsilon} + [\ln |r| f(\beta)]_E^{\varepsilon} \} + \text{C.P.V.} \\ &= \lim_{\varepsilon \rightarrow 0} \{ -\ln(\varepsilon) [f(\alpha) + f(\beta)] + \ln(r_E) f(\beta) + \ln(r_D) f(\alpha) \} + \text{C.P.V.} \end{aligned} \tag{106}$$

Here,  $r_E$  and  $r_D$  are distances between the source point and points  $E$  and  $D$ , respectively. C.P.V. denotes Cauchy principal value terms which arise out of the integral  $I_5$ . It so happens that, when eqn (90) is considered as a whole, all Cauchy principal value terms arising out of the singular kernels  $v_{jp,i}^*$  and  $t_{jp}^*$  cancel out and hence, in effect, there are no free terms arising out of the line integrals in eqn (90). Therefore, it is sufficient to consider eqn (106) without the C.P.V. terms.

Since  $EOD$  is a straight line (Fig. 2),

$$\beta = \alpha + \pi. \tag{107}$$

Hence, from eqns (103) and (107) it is clear that

$$f(\alpha) + f(\beta) = 0. \tag{108}$$

Therefore, eqn (106) takes the following form

$$I_5 = \ln\left(\frac{r_D}{r_E}\right) \cdot f(\alpha). \tag{109}$$

The above mentioned procedure of regularizing the singular integral is explained in the context of a two-dimensional problem for the  $v_{jp,k}^*$  kernels. It should be noted here that the kernels  $n_k E_{ijmn} v_{jp,i}^*$  and  $t_{jp}^* (= n_k E_{ijkl} v_{jp,j}^*)$  appearing in eqn (110) will have a similar procedure of regularizing the singular integrals, since the component of the normal  $n_k$  (or  $n_q$ ) are constant over the straight line  $EOD$  (Fig. 2). Without any loss of generality a similar procedure could be adopted in the context of three-dimensional problems as well.

1.6.4. *Regularization of domain integrals.* As seen from eqns (89) and (90) both the velocity and velocity gradient expressions involve Cauchy principal value integrals in the domain. For illustrative purposes, let us consider the integral

$$J_1 = \int_{\Omega} E_{ijmn}^{(e)} D_{mn}^{(p)}(x_m) v_{jp,ik}^*(x_m, \xi_m) d\Omega, \tag{110}$$

we may write  $v_{jp,ik}^*$  (for two-dimensional problems) as:

$$v_{jp,ik}^* = \frac{\Psi(\theta)}{r^2}. \tag{111}$$

Here,  $r$  is the distance between the source point and field point.  $\theta$  is the angle made by the line connecting the source and field points with the  $x$ -axis. Due to the inherent property of  $\Psi(\theta)$  it could be seen that

$$\int_0^{2\pi} \Psi(\theta) d\theta = 0. \tag{112}$$

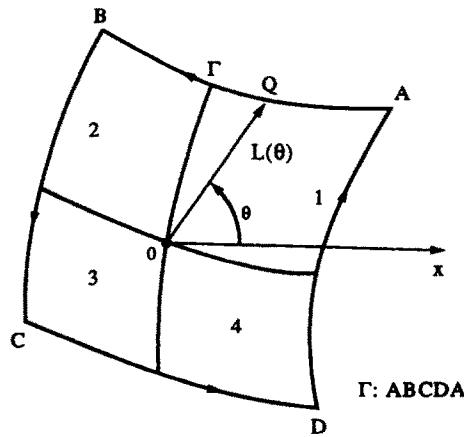


Fig. 3. Numerical evaluation of singular domain integral when source point is in the interior.

As in Fig. 3, let us consider a set of neighboring elements such that the source point is located at  $O$ . This scenario could be considered as a general situation when the source point lies in the interior. Introducing shape functions into eqn (110) and extracting out the singularity (procedure adopted, is similar to the case of line integrals [eqn (102)]), the resulting singular integral would become

$$J_2 = \int_{\Omega} v_{jp,ik}^* d\Omega. \tag{113}$$

Integrating  $v_{jt,ik}^*$  in all the neighboring elements (Fig. 3) of the source point, eqn (113) turns out to be

$$\begin{aligned} J_2 &= \sum_{l_e=1}^4 \int_{\Omega_{l_e}} \frac{\Psi(\theta)}{r^2} d\Omega \\ &= \lim_{\epsilon \rightarrow 0} \int_0^{2\pi} \int_{\epsilon}^{R(\theta)} \frac{\Psi(\theta)}{r^2} r dr d\theta. \end{aligned} \tag{114}$$

Here  $R(\theta)$  is defined in Fig. 3. Making use of the property of the functional in eqn (112) we could reduce the above mentioned integral into a regular integral as follows

$$J_2 = \int_0^{2\pi} \Psi(\theta) \ln |R(\theta)| d\theta. \tag{115}$$

Let us next consider the scenario when the source point is on a smooth part of the boundary (Fig. 4). Introducing shape functions and extracting out the singularity in eqn (110), the singular integral turns out to be

$$J_3 = \int_{\Omega_{E_1} + \Omega_{E_2}} v_{jp,ik}^* d\Omega. \tag{116}$$

Applying the divergence theorem to the non-singular region  $(\Omega_{E_1} + \Omega_{E_2} - \epsilon)$  (Fig. 4) we have

$$\begin{aligned} J_3 &= \lim_{\epsilon \rightarrow 0} \left[ \int_{\Gamma} n_i v_{jp,k}^* d\Gamma + \int_{\partial\epsilon} n_i^* v_{jp,k}^* d\Gamma + \int_{\epsilon} v_{jp,ki}^* d\epsilon \right] \\ &= J_4 + J_5 + J_6. \end{aligned} \tag{117}$$

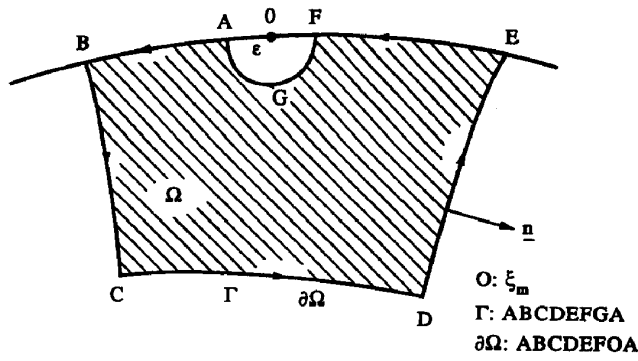


Fig. 4. Numerical evaluation of singular domain integral when source point is on a smooth part of the boundary.

Upon further analysis it is clear that  $J_4$  gives rise to a Cauchy principal value line integral, which would then be evaluated by a similar procedure discussed for line integrals in the previous section.  $J_5$  gives rise to free terms arising out of the singular integrals in the domain, which were already taken into consideration in eqn (90) and taking the appropriate limiting values  $J_6$  can be shown to be zero.

1.6.5. *Numerical results and discussion.* The problem of a thick cylinder under prescribed internal radial velocity is considered for illustrative purposes. The dimensions, material properties, and boundary conditions are given in Fig. 5(a). Since the problem is symmetric about the angular direction, a  $20^\circ$  section [Fig. 5(b)] is considered for convenience, with appropriate boundary conditions. Three different meshes (of progressive mesh refinement) were considered (Fig. 6) for the analysis. A small deformation analysis (up to 1% radial

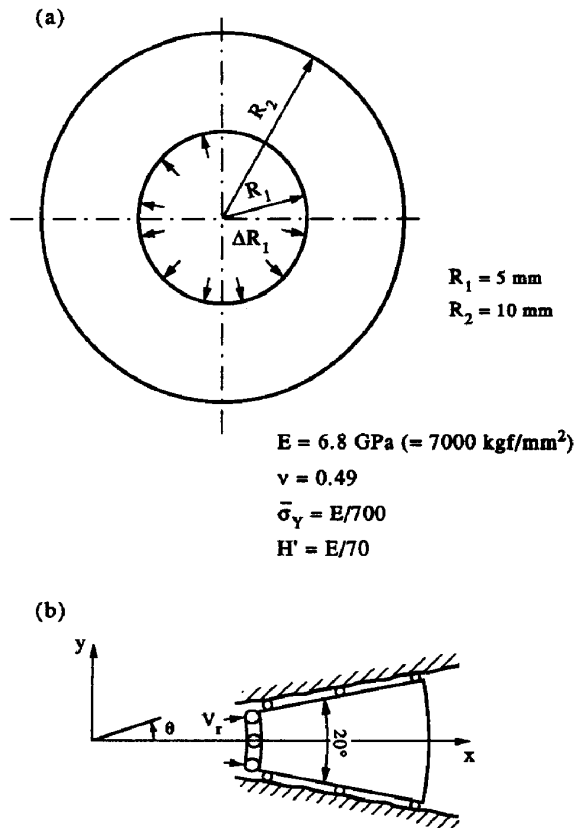
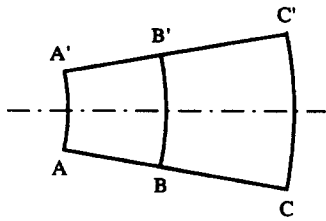
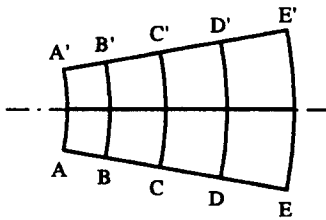


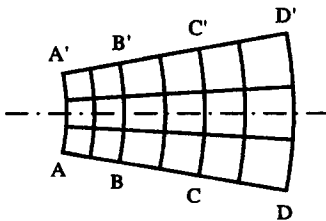
Fig. 5. Expansion of a thick cylinder under prescribed internal velocity.



(1) Mesh 1 7 B.E. and 2 D.E.



(2) Mesh 2 12 B.E. and 8 D.E.



(3) Mesh 3 18 B.E. and 18 D.E.

Fig. 6. Boundary and domain mesh discretizations.

expansion at the inner radius) was considered as a first step to ascertain the nature of convergence and accuracy of both formulations. The solutions obtained by using the field-boundary element method are compared with those designated as direct solution. The direct solutions were obtained by direct step-by-step integrations of the kinematic quantities and the elastoplastic constitutive equation, assuming the material to be incompressible (Poisson's ratio is set to be 0.5). As seen in Figs 7, 8 and 9, the present formulation gives accurate results, even with a coarse mesh. As for the standard formulation the results progressively improve as the mesh is refined.

Next, a large deformation analysis was performed with the same mesh discretizations given in Fig. 8. Radial deformations up to 30% were considered. As seen in Fig. 10, the present method gave somewhat acceptable results when the standard formulation failed to even generate results due to numerical degradation for Mesh 1. The results for the subsequent meshes improve with mesh refinement (Figs 11 and 12). In all cases considered, the present method yields more accurate results than the standard formulation. The present method, based on a direct integral representation of velocity gradients, which are of the nonhyper-singular type at the boundary, leads to much better numerical results for boundary stress rates than the conventional method where in the integral representations for velocities is differentiated to obtain deformation rates and stress-rates. This improvement in numerical accuracy of the present method over the conventional method could be attributed to the two tier system of evaluation of velocity gradients in the conventional methods.

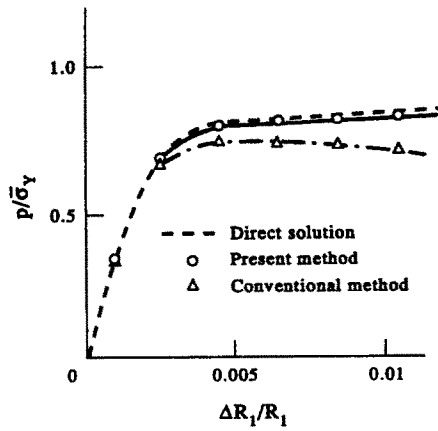


Fig. 7. Pressure-radial displacement curve. (Mesh 1, small deformation analysis).

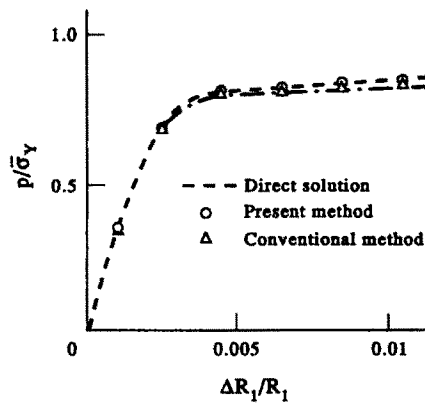


Fig. 8. Pressure-radial displacement curve. (Mesh 2, small deformation analysis).

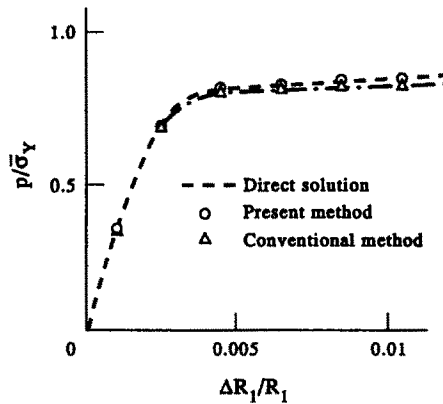


Fig. 9. Pressure-radial displacement curve. (Mesh 3, small deformation analysis).

## 2. A FULL TANGENT STIFFNESS FIELD-BOUNDARY ELEMENT FORMULATION FOR GEOMETRIC AND MATERIAL NON-LINEAR PROBLEMS OF SOLID MECHANICS

The analysis of the field-boundary element method for geometric and material non-linear problems in solid mechanics is generally carried out by an incremental algorithm, where the solution methodology employed is first to obtain velocities (or displacement increments) through an integral relationship. The velocity gradients on the boundary are

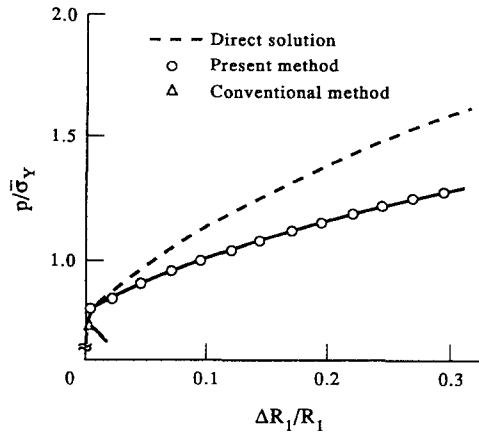


Fig. 10. Pressure-radial displacement curve. (Mesh 1, large deformation analysis).

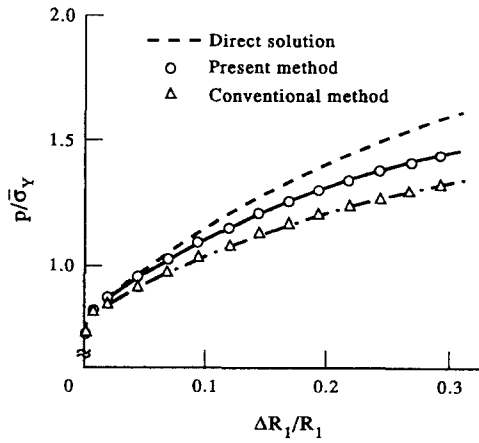


Fig. 11. Pressure-radial displacement curve. (Mesh 2, large deformation analysis).

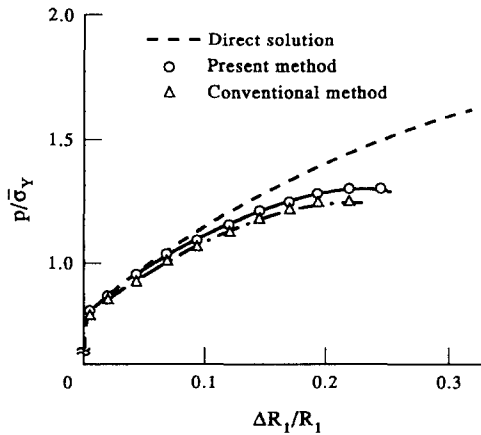


Fig. 12. Pressure-radial displacement curve. (Mesh 3, large deformation analysis).

then obtained through an integral relationship or a boundary stress-strain-rate (see the previous section) algorithm. Once the boundary variables are completely determined, the velocities and velocity gradients at the interior are evaluated by taking the source point in their respective integral equations to the desired interior location. Such an initial strain iteration algorithm is, in general, insensitive to the initial stress velocity gradient coupling

terms (in the domain integrals), which play a dominant role in problems which involve bifurcation phenomena (buckling, diffused necking, etc.) in its solution path. Hence, the convergence may be unacceptably slow or the bifurcation phenomena may be completely ignored when initial strain type iteration methods were to be employed to solve such problems.

The initial stress velocity gradient coupling terms (i.e.  $\tau_{kj}v_{i,k}$  terms) need to be properly accounted for in the calculation of velocities (or displacement increments) for problems which involve bifurcation phenomena. For this purpose, a full tangent stiffness field-boundary element formulation is presented. Unlike in the initial strain approach, in the full tangent stiffness approach, the velocity field in the entire domain of the body is assumed as a primary variable and the velocity gradients are expressed through the differentiated shape functions and nodal velocities in the domain elements. Hence a system of equations involving all non-linear effects in terms of velocities in the form of a tangent stiffness matrix is obtained. In this section, a tangent stiffness field-boundary element formulation is presented for elastoplastic solids undergoing large strains. A generalized mid-point radial return algorithm is used for determining the objective increments of stress from the computed velocity gradients. Moreover, a mid-point evaluation of the generalized Jaumann integral is used to determine the material increments of stress. The constitutive equation employed (the one chosen is for illustrative purposes only) for the analysis is based on an endochronic model of combined isotropic/kinematic hardening finite plasticity using the concepts of a material director triad and the associated plastic spin. The problem of diffused necking instability of a plate subjected to uniform tension is analyzed using the initial strain and the full tangent stiffness field-boundary element algorithms. Both initially perfect plates, as well as those containing initial imperfections, are analysed. The superiority of the full tangent stiffness algorithm, in capturing the bifurcation phenomena is demonstrated when the plastic instabilities are analysed.

### 2.1. Field-boundary element equation formulation

Although the integral equation representation for the velocity in finite strain elastoplasticity has previously been presented, the nature of the integral equation in such a case is discussed here. The integral representation for the velocity  $v_q$  is written as,

$$C_{pq}v_q(\xi_m) = \int_{\partial\Omega} \{ \dot{t}_j v_{jp}^*(x_m, \xi_m) - t_{jp}^*(x_m, \xi_m) v_j \} d(\partial\Omega) + \int_{\Omega} \dot{b}_j v_{jp}^*(x_m, \xi_m) d\Omega \\ + \int_{\Omega} \{ E_{ijkl} D_{kl}^P + \tau_{ik} (W_{kj} - W_{kj}^P) - (W_{ik} - W_{ik}^P) \tau_{kj} + v_{i,k} \tau_{kj} \} v_{jp,i}^*(x_m, \xi_m) d\Omega. \quad (118)$$

Here, when  $\xi_m$  is a smooth boundary point ( $\xi_m \in \partial\Omega$  smooth),  $C_{pq} = \frac{1}{2}\delta_{pq}$  and when  $\xi_m$  is an interior point ( $\xi_m \in \Omega$ ),  $C_{pq} = \delta_{pq}$ . The nature of the integral equation (118) is examined as follows. The first term on the right-hand side of eqn (118), involving only a boundary integral, corresponds to the linear elastic behavior of the material in its current state. The second term, involving a domain integral, accounts for the body forces, but still corresponds to linear elastic behavior in the current state. The third term on the right-hand side of (118), involving a domain integral, contains the crux of the finite strain elastic-plastic problem : (i) the term  $E_{ijkl} D_{kl}^P$  accounts for the effects of plastic strain-rate, (ii) the terms such as  $\tau_{ik} W_{kj}^P$  etc. account for the effects of plastic spin, and (iii) the term  $v_{i,k} \tau_{kj}$  accounts for the coupling for initial stresses in the current configuration with the additional deformation from the current configuration (this term plays a dominant role in problems of buckling, instability, etc.). If only the first term on the right-hand side is used in any discretization process, and the domain integral terms are used only in an iterative process, one is led to the so-called ‘‘initial strain’’ iteration approach, based on the so-called ‘‘linear elastic stiffness matrix’’. Such an iterative technique is shown in the present section, to fail in the case of plastic instability problems. If all the terms on the right-hand side of eqn (118) are simultaneously used in a discretization process, one is led to the so-called ‘‘full tangent stiffness’’ method. It is also seen that this tangent stiffness method involves trial functions

$v_i$  not only at the boundary  $\partial\Omega$  but also in the domain  $\Omega$ . These concepts of “initial strain” and “tangent stiffness” field-boundary element methods were discussed by Atluri (1984). The  $v_{ip}^*$ ,  $t_{ip}^*$  and  $v_{jp,i}^*$  kernels for the case of two-dimensional plane strain are defined as follows:

$$\begin{aligned}
 y_i &= x_i - \xi_i, \quad r = \sqrt{(x_i - \xi_i)(x_i - \xi_i)} \\
 v_{ip}^*(x_m, \xi_m) &= \frac{1}{8\pi\mu(1-\nu)} \left\{ (3-4\nu) \ln\left(\frac{1}{r}\right) \delta_{ip} + \frac{y_i y_p}{r^2} \right\} \\
 t_{ip}^*(x_m, \xi_m) &= \frac{-1}{4\pi(1-\nu)r} \left[ \frac{n_k y_k}{r} \left\{ (1-2\nu) \delta_{ip} + 2 \frac{y_i y_p}{r^2} \right\} \right. \\
 &\quad \left. - (1-2\nu) \left( \frac{y_p}{r} n_i - \frac{y_i}{r} n_p \right) \right] \\
 v_{jp,i}^*(x_m, \xi_m) &= \frac{1}{8\pi\nu(1-\nu)r} \left\{ -(3-4\nu) \frac{y_i}{r} \delta_{pj} + \left( \delta_{ip} \frac{y_j}{r} + \delta_{ij} \frac{y_p}{r} \right) - 2 \frac{y_i y_j y_p}{r^3} \right\}. \quad (119)
 \end{aligned}$$

Here,  $n_k$  are the components of the unit outward normal to the boundary at  $x_m$ , and  $\mu$  and  $\nu$  are the shear modulus and the Poisson's ratio, respectively. It is seen that the test functions  $v_{ip}^*$  and  $t_{ip}^*$  remain unchanged during the entire elastic-plastic deformation path, and correspond to the initial elastic state of the solid. Further,  $v_{ip}^*$  remains symmetric under  $i \rightarrow p$  interchange, while  $t_{ip}^*$  has a skew-symmetric component under  $i \rightarrow p$  interchange. It is seen that if the material is incompressible even in its initial elastic state ( $\nu = \frac{1}{2}$ ), the kernel  $t_{ip}^*$  in fact becomes simpler in as much as its skew-symmetric part tends to zero. Also, as plastic flow fully develops, the rate of deformation is nearly incompressible, i.e.  $v_i$  satisfy the condition that  $v_{i,i} = 0$ . From eqn (118) it can be examined that this potential constraint condition on  $v_i$  does not pose any “locking” problems. This is not the case in symmetric Galerkin-type finite element formulations, wherein, in a pure displacement approach for finite strain plasticity, the appropriate functionals (and weak forms) involve terms of the type  $(\lambda v_{i,i} v_{j,j})$  where  $\lambda$  is the bulk modulus [see Atluri (1979, 1980)]. For a typical material, the magnitude of the elastic moduli,  $E_{ijkl}$  in eqn (118), is expected to be much larger than that of  $\tau_{ij}$  (about 2 orders of magnitude). This difference is not as severe as that between  $E_{ijkl}^i$  and  $\lambda$ , as in the finite element formulation. This is the primary reason as to why “locking” does not occur in the field-boundary element method. However, the term  $\tau_{kj} v_{i,k}$  plays a central role in eqn (118), in altering the stiffness of the structure at bifurcation.

## 2.2. Numerical implementation of a full tangent stiffness field-boundary element method

In the “initial strain” type field-boundary element method, the velocities and boundary traction rates are solved first through an integral equation for velocities on the boundary (i.e. by discretizing the first term on the right-hand side of eqn (118) only, assuming that the body forces are zero). Then the velocity gradients on the boundary are solved either by the boundary stress-strain algorithm or by an integral representation. The velocity and velocity gradients in the interior are solved next by integral representations. Then, the rate of plastic strain and other material parameters are determined. An iterative initial strain type algorithm is carried out till all the field parameters converge. Such an algorithm is not very sensitive to the initial stress velocity gradient coupling (i.e. the  $\tau_{kj} v_{i,k}$ ) term and will not be suitable for problems involving bifurcation phenomena.

To avoid such a predicament, in the “tangent stiffness” field-boundary element method, we assume the velocity field as a primary variable not only on the boundary but also in the interior of the body. The velocity gradients can be expressed by differentiating the shape functions associated with the nodal velocities in the interior elements. Thus, all material and geometric non-linear effects are directly accounted for in the field-boundary integral equation for velocities throughout the domain. Furthermore, a tangent stiffness matrix can be obtained with known or unknown surface traction rates, as well as velocities through-



out the domain. [See Banerjee and Reveendra (1987), for an analogous method in small strain plasticity.]

In the following subsections, numerical implementations of the integral equations for the present full tangent stiffness field-boundary element method are discussed for a two-dimensional plane strain case.

2.2.1. *Boundary integrals.* Three-noded quadratic isoparametric boundary elements are used to discretize the surface of the body. Let  $N_I^B$  ( $I = 1, 2, 3$ ) be a shape function associated with the  $I$ th nodal point in a boundary element. Let  $v_I^t$  and  $t_I^t$  ( $I = 1, 2, 3$ ) be a nodal velocity vector and traction vector at the  $I$ th nodal point in a boundary element. Thus, the boundary integral in eqn (118) is given by the following discretization

$$\int_{\partial\Omega} (v_{jp}^* t_j - t_{jp}^*) d(\partial\Omega) = \sum_{IB=1}^{NBE} \left[ \sum_{I=1}^3 \left\{ t_j^t \int_{\partial\Omega_E} N_I^B v_{jp}^* d(\partial\Omega_E) - v_j^t \int_{\partial\Omega_E} N_I^B t_{jp}^* d(\partial\Omega_E) \right\} \right] \quad (120)$$

where,  $NBE$  is the total number of boundary elements.

2.2.2. *Domain integrals.* Eight-noded isoparametric elements are used here. Stress components, plastic strain, and plastic spin evolution equations are evaluated at four points (sampling points) in each domain element (see Fig. 13). Thus, the stress components, plastic strain, and plastic spin evolution equations are interpolated to any other location from their sampling points, by using the Lagrange interpolation functions. Let  $\hat{N}^I$  ( $I = 1, 2, 3, 4$ ) be the Lagrange interpolation function associated with the  $I$ th stress point in a domain element. Then,

$$\begin{aligned} C_{ijkl}(\xi, \eta) &= \sum_{I=1}^4 \hat{N}^I(\xi, \eta) C_{ijkl}(\xi_I, \eta_I) \\ \tau_{ij}(\xi, \eta) &= \sum_{I=1}^4 \hat{N}^I(\xi, \eta) \tau_{ij}(\xi_I, \eta_I), \end{aligned} \quad (121)$$

where,  $C_{ijkl}$  represents the tensor in the plastic strain evolution equation

$$D_{ij}^P = C_{ijkl} D_{kl}, \quad C_{ijkl} = \frac{1}{C} N_{ij} N_{kl}.$$

Hence, the stress components and plastic strain evolution equations could be expressed in

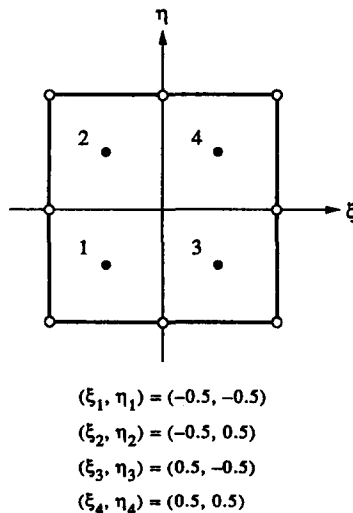


Fig. 13. Eight-noded isoparametric element used for volume discretization.

this manner everywhere in the domain. Also, by using the shape functions  $N_I$  ( $I = 1, 2, \dots, 8$ ) of eight-noded isoparametric elements, the velocity and the velocity gradients can be expressed as follows

$$\begin{aligned}
 v_i(\xi, \eta) &= \sum_{I=1}^8 N_I^p(\xi, \eta) v_i(\xi_I, \eta_I) \\
 \frac{\partial v_i(\xi, \eta)}{\partial x_j} &= \sum_{I=1}^8 \left( \frac{\partial \xi}{\partial x_j} \frac{\partial N_I^p}{\partial \xi} + \frac{\partial \eta}{\partial x_j} \frac{\partial N_I^p}{\partial \eta} \right) v_i(\xi_I, \eta_I).
 \end{aligned}
 \tag{122}$$

The domain integral in eqn (118) is therefore expressed by the following expressions (in the absence of body force)

$$\begin{aligned}
 D.I. &= \int_{\Omega} \{ E_{ijkl} D_{kl}^p + \tau_{ik} (\overline{W}_{kj} - W_{kj}^p) - (W_{ik} - W_{ik}^p) \tau_{kj} + v_{i,k} \tau_{kj} \} v_{j,p,i}^* \, d\Omega \\
 &= \int_{\Omega} A_{ijkl} v_{k,l} v_{j,p,i}^* \, d\Omega \\
 &= \sum_{ID=1}^{NDE} \left\{ \sum_{J=1}^8 \sum_{K=1}^4 A_{ijkl}(\xi_J, \eta_J) v_k(\xi_I, \eta_I) \right. \\
 &\quad \left. \times \int_{\Omega_E} \hat{N}_J(\xi, \eta) \left( \frac{\partial \xi}{\partial x_l} \frac{\partial N_I^p}{\partial \xi} + \frac{\partial \eta}{\partial x_l} \frac{\partial N_I^p}{\partial \eta} \right) v_{j,p,i}^* \, d\Omega_E \right\} \\
 &= \sum_{ID=1}^{NDE} \left\{ \sum_{J=1}^8 K_{kp}^I v_k(\xi_I, \eta_I) \right\},
 \end{aligned}
 \tag{123}$$

where,  $A_{ijkl}$  (in the absence of plastic spin, for simplicity), is written† as

$$A_{ijkl} = E_{ijmn} \left( \frac{1}{C} N_{mn} N_{kl} \right) + \frac{1}{2} \tau_{im} \delta_{jn} (\delta_{mk} \delta_{nl} - \delta_{nk} \delta_{ml}) - \frac{1}{2} \delta_{in} (\delta_{nk} \delta_{ml} - \delta_{nk} \delta_{nl}) \tau_{mj} + \delta_{ik} \tau_{lj}, \tag{124}$$

where,  $NDE$  is the total number of domain elements,  $K_{kp}^I$  is termed the domain element stiffness matrix for the source point  $\xi$ . It is important to note that, unless the geometry is updated, we need not recompute domain integrals, because the initial stress and the plastic strain evolution equation are given pointwise, outside of the integral [eqn (123)].

2.2.3. *Matrix formulation.* A system of linear equations can be obtained through the discretized equations [eqns (120) and (123)] given in the previous section. Using the process of collocation, and by taking each nodal point to be a source point ( $\xi_m$ ), a sufficient number of linear equations is generated. These are shown in matrix form as,

$$[T^*] \{v\} = [U^*] \{i\}. \tag{125}$$

Let  $N$  be the total number of nodal points (both on the boundary and in the interior), and let  $M$  be the total number of boundary nodal points only. Then  $\{v\}$  is the vector of nodal velocities ( $N \times 1$ ), and  $\{i\}$  is the vector of nodal tractions ( $M \times 1$ ).  $[T^*]$  and  $[U^*]$  are the coefficient matrices, which depend on the initial stresses, etc. [see eqns (120) and (123)]. To solve for unknown nodal values, known and unknown variables are rearranged appropriately such that, one is led to a system of equations

$$[K] \{x\} = \{y\} \tag{126}$$

† Here we consider only the case of isotropic hardening, for simplicity, and without loss of any generality.

where,  $[K]$  is the tangent stiffness matrix, and  $\{x\}$  and  $\{y\}$  are the unknown and the load vector respectively. The unknown vector is obtained by,

$$\{x\} = [K]^{-1} \{y\}. \quad (127)$$

**2.2.4. Numerical quadrature scheme.** Since isoparametric elements are considered, closed form evaluation of the integrals in eqn (118) is not possible. Hence, numerical quadrature schemes which accurately evaluate both boundary and domain integrals of eqn (118) are presented below. As for the boundary integrals, the 10 Gauss point quadrature formula is employed for all non-singular cases, and the logarithmic weighted 7 Gauss point formula is used for logarithmic singular cases [see Stroud (1966)]. The  $1/r$  singular integral associated with the Cauchy principal value is evaluated by the use of the rigid body modes.

The kernel functions  $v_{j,p,i}^*$  that are present in the domain integral have the structure  $(1/r)f(\cos \theta, \sin \theta)$ . Here,  $r$  is the distance between a field point  $x_m$  and a source point  $\xi_m$ , and  $\theta$  is the angle made by the line joining  $x_m$  and  $\xi_m$  with the  $x_1$  axis

$$\left( \theta = \tan^{-1} \frac{x_2 - \zeta_2}{x_1 - \zeta_1} \right).$$

When the field point falls within a set of field elements immediately surrounding the source point, the  $(1/r)$  singularity in the integrand is cancelled with the  $(r \, dr \, d\theta)$  term of the Jacobian and mapping the elements appropriately. On the other hand, the  $f(\cos \theta, \sin \theta)$  part is considered to have steeper variation than the  $1/r$  part, when the distance between a source point and a field element is small compared with the element size. Thus, for this group of field elements, we choose a numerical quadrature based on the maximum angular variation in a domain element, which is determined as shown in Fig. 14. It is noted that the non-product formulas [Stroud (1971)], as well as the standard product Gauss formulas, are employed for the domain integral.

### 2.3. Solution algorithm

A non-iterative full tangent stiffness method is employed in the analysis of finite strain elastoplasticity, with the mid-point radial return algorithm and an objective stress integration scheme. The mid-point radial return algorithm and the objective stress integration scheme introduced in this section are quite effective for the non-iterative finite strain elastic-plastic calculation. These algorithms can prevent unreasonably small time increments, generally required in non-iterative elastic-plastic calculations. Moreover, they can also give a more accurate solution to the analysis. These algorithms have previously been discussed.

### 2.4. Numerical example: diffused necking of a tensile plate and discussion

The plastic instability problem of diffuse necking of a tensile bar is analysed as a numerical example. Here, rectangular elastic-plastic plates are subjected to tensile deformation (in plane strain) with shear free end conditions, as shown in Figs 15(a, b). Two different solution techniques are employed here. One is the present full tangent stiffness method, and the other is an initial strain iteration method. The results obtained by these

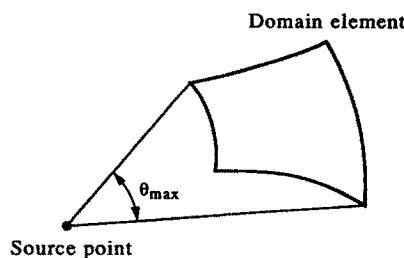
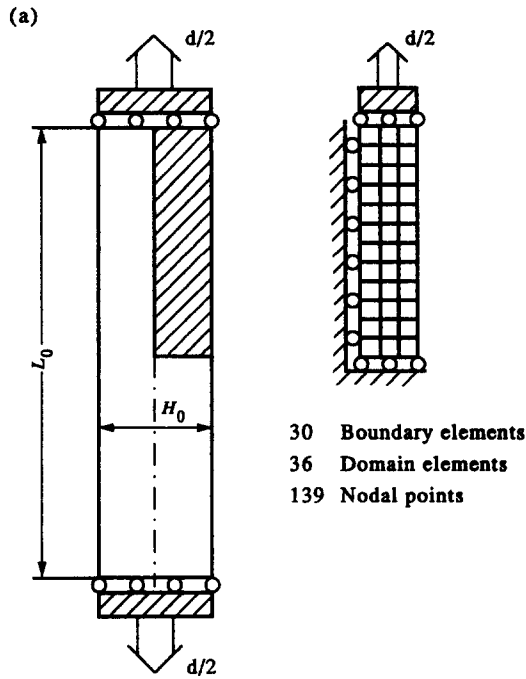
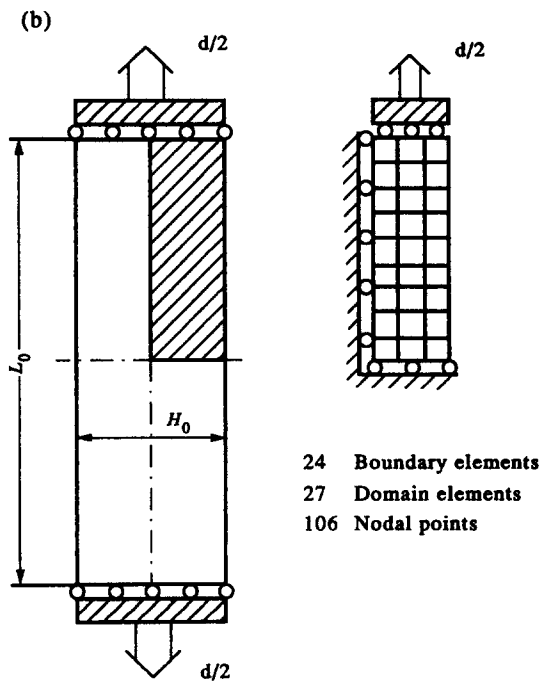


Fig. 14. Maximum angular variation in a domain element.



**Mesh discretization and boundary conditions  
for case 1 ( $L_0/H_0 = 4$ )**

Fig. 15(a). Specimens for analyses of diffused necking and their field-boundary element mesh discretizations (case 1).



**Mesh discretization and boundary conditions  
for case 2 ( $L_0/H_0 = 3$ )**

Fig. 15(b). Specimens for analyses of diffused necking and their field-boundary element mesh discretizations (case 2).

Table 1. Material properties employed to the analysis

Young's modulus $E$	$6.895 \times 10^4$ MPa
Poisson's ratio $\nu$	0.49
Yield stress $\sigma_y$	344.75 MPa
One dimensional stress-strain relationship	
$\epsilon = \sigma/E$	$\sigma \leq \sigma_y$
$\epsilon = \sigma^N/(E\sigma_y^{N-1})$	$\sigma \geq \sigma_y$
$N = 8$	

methods are compared (for the load and the diffused necking bifurcation point) with the direct analytical method [see Okada *et al.* (1990)]. The boundary value problems shown in Figs 15(a, b) are considered here. As shown in Fig. 15, the case (1) and the case (2) have their initial aspect ratios as  $(H_0/LI_0)^{1/4}$  and  $1/3$ , respectively. Shear free displacement boundary conditions are specified at both ends of tensile plate. Mesh discretizations and boundary conditions for the field-boundary element analysis are also shown in Fig. 15. From symmetry considerations, one-fourth of the actual problem is analysed. Material properties used in the analysis are given in Table 1. A power law hardening elastic-plastic material is considered here. The analysis is carried out under plane strain conditions. In Figs 16 and 17, the solutions obtained by an initial strain iteration field-boundary element method are first presented for the case (1), wherein initial aspect ratio is  $1/4$ . Two different types of tensile bars are considered here: one has a perfect initial geometry and the other has an initial geometric imperfection of 1% in the width of the tensile plate at its mid-length. The solution for the case without initial imperfections traces over on the fundamental homogeneous

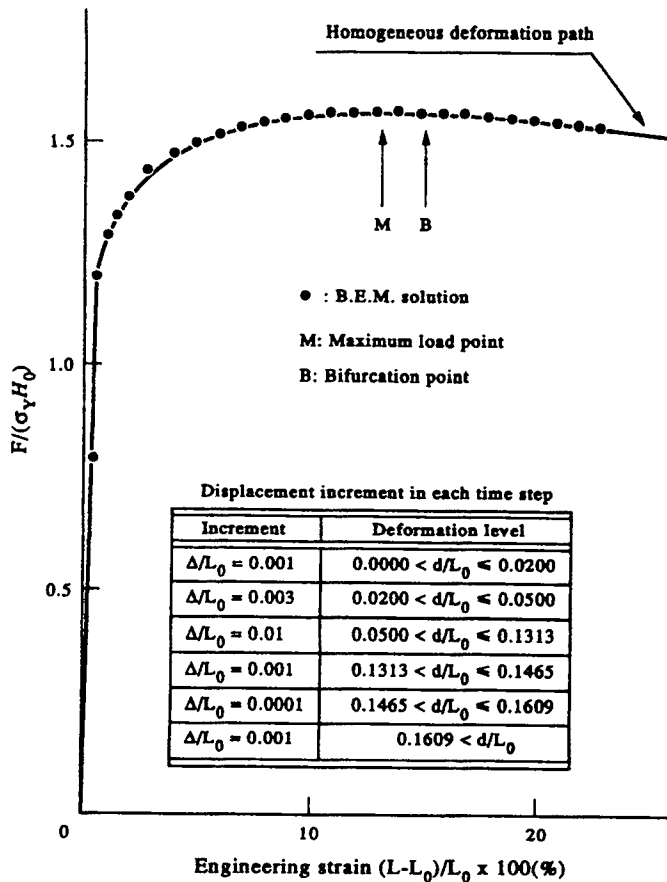


Fig. 16. Normalized load-engineering strain curve for the case 1. (Analysed by a conventional initial strain iteration field-boundary element algorithm, without initial geometric imperfections.)

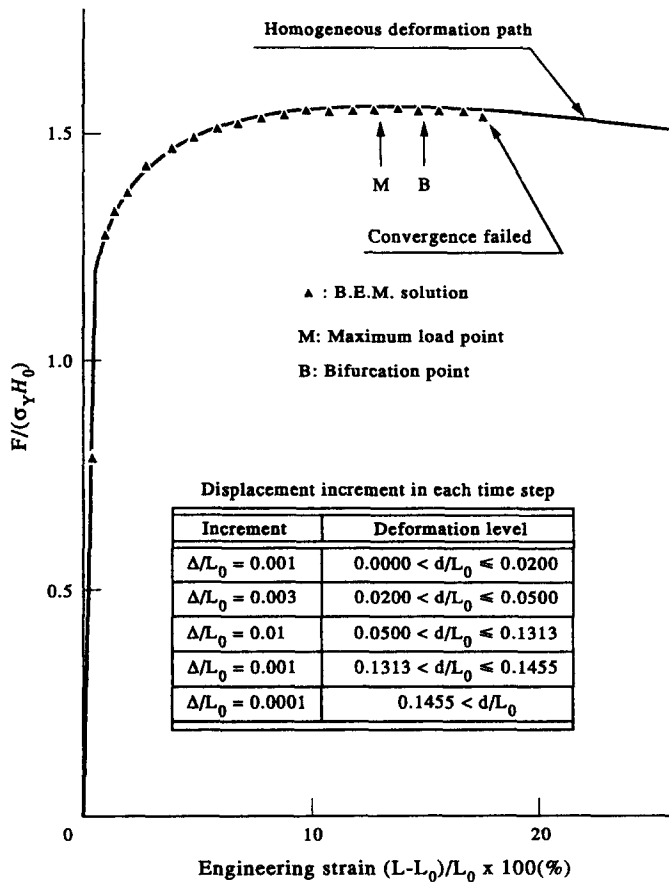


Fig. 17. Normalized load–engineering strain curve for the case 1. (Analysed by a conventional initial strain iteration field-boundary element algorithm, with 1% of geometric initial imperfection.)

deformation path obtained by the direct method. In the case with an initial geometric imperfection, the solution (by the initial strain iteration method) fails to converge after the bifurcation point. These numerical results clearly indicate that either the plastic instability is ignored or the convergence fails, when an initial strain type iterative algorithm is used.

The same problem is successfully analysed by using the present full tangent stiffness field-boundary element approach. The analysis is carried out without any initial geometric imperfections when using the tangent stiffness method. The normalized load–engineering strain curves are shown in Figs 18 and 19, for the cases 1 and 2, wherein the initial aspect ratios are  $\frac{1}{4}$  and  $\frac{1}{3}$ , respectively. It is seen that the load vs engineering strain curve obtained by the full tangent stiffness method traces over that of the fundamental homogeneous deformation path up to the bifurcation point, and drops gradually thereafter. This type of behavior in the load–engineering strain curves corresponds to the diffused necking deformation mode. The displacement increment  $\Delta$  in each incremental time step is controlled carefully, as shown in the Figs 16–19, with respect to the level of engineering strain. The deformed mesh configurations are shown in Figs 20(a, b) at the engineering strains of 15.3% and 20.3%, respectively, for the case 1 (i.e. of initial aspect ratio  $\frac{1}{4}$ ). It is seen that the deformation is homogeneous up to the bifurcation point (engineering strain 15.3%), and diffused necking develops thereafter. The deformed mesh configurations at the engineering strains 17.2% and 20.7% are shown in Figs 21(a, b), for case 2 (i.e. of initial aspect ratio  $\frac{1}{3}$ ). The same trend is observed in the solution for case 2 (engineering strain at the bifurcation point is 17.1%). A further discussion of the analysis (by the full tangent stiffness method) is illustrated with the distributions of relative rate of equivalent plastic strain and equivalent plastic strain. The relative rate of plastic strain  $\dot{\epsilon}_R^P$  is defined by,

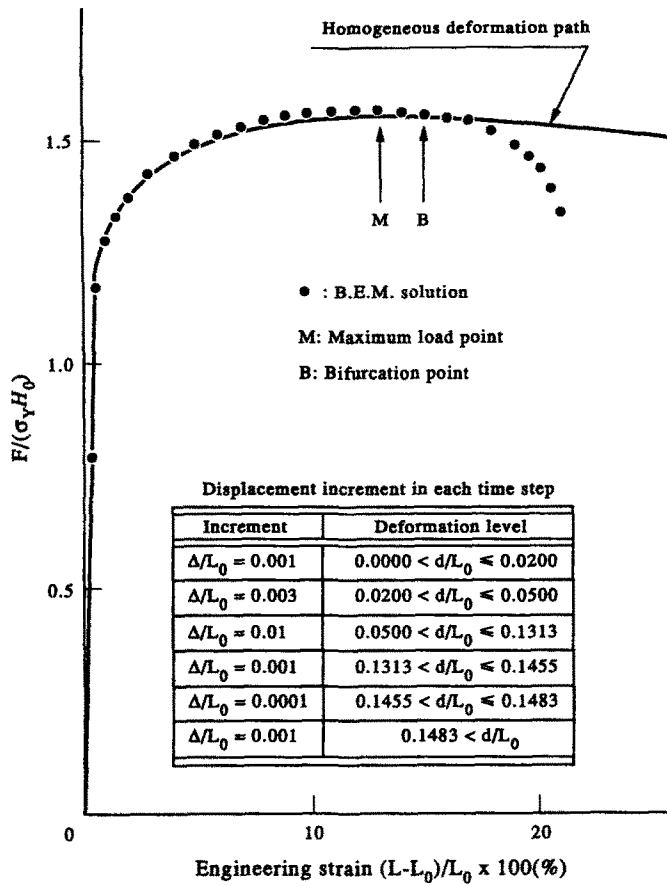


Fig. 18. Normalized load-engineering strain curve for the case 1 (Analysed by present full tangent stiffness field-boundary element approach.)

$$\dot{\bar{\epsilon}}_R^P = \left( \frac{\dot{\epsilon}_{ij}^P}{2 \frac{l}{\sqrt{3}} \dot{l}} \right) \tag{128}$$

and

$$\dot{\bar{\epsilon}}^P = \sqrt{\frac{2}{3}} (\dot{\epsilon}_{ij}^P \dot{\epsilon}_{ij}^P)^{1/2}. \tag{129}$$

Here,  $\dot{\epsilon}_{ij}^P$  is the rate of plastic strain,  $l$  is the current length of the plate and  $\dot{l}$  is its time derivative. When a rigid plastic plate is undergoing homogeneous stretching under plane strain conditions, the relative rate of equivalent plastic strain  $\dot{\bar{\epsilon}}_R^P$  is always equal to one. The equivalent plastic strain is defined as

$$\bar{\epsilon}^P = \sqrt{\frac{2}{3}} (\epsilon_{ij}^P \epsilon_{ij}^P)^{1/2}, \tag{130}$$

where,  $\epsilon_{ij}^P$  is plastic strain. The distribution of relative rate of plastic strain at the engineering strains 14.5%, 15.3%, 17.8% and 19.3% are shown in Figs 22(a), (b), (c) and (d), for the case 1. These figures show the development of the diffused necking deformation mode and the elastic unloading zone ( $\dot{\bar{\epsilon}}_R^P = 0$ ) in the plate. At an engineering strain of 19.3% (as the deformation proceeds) the distribution of  $\bar{\epsilon}^P$  seems to concentrate at the portion of necking (Fig. 23). Moreover,  $\dot{\bar{\epsilon}}_R^P$  and  $\bar{\epsilon}^P$  at the engineering strain of 19.3% [Figs 22(c) and 23] seem to indicate high concentration of plastic deformation around a 50° section across the diffused necking portion of tensile plate. This behavior corresponds to a shear band type deformation. The same trend is seen in the solution for the case 2 whose initial aspect ratio

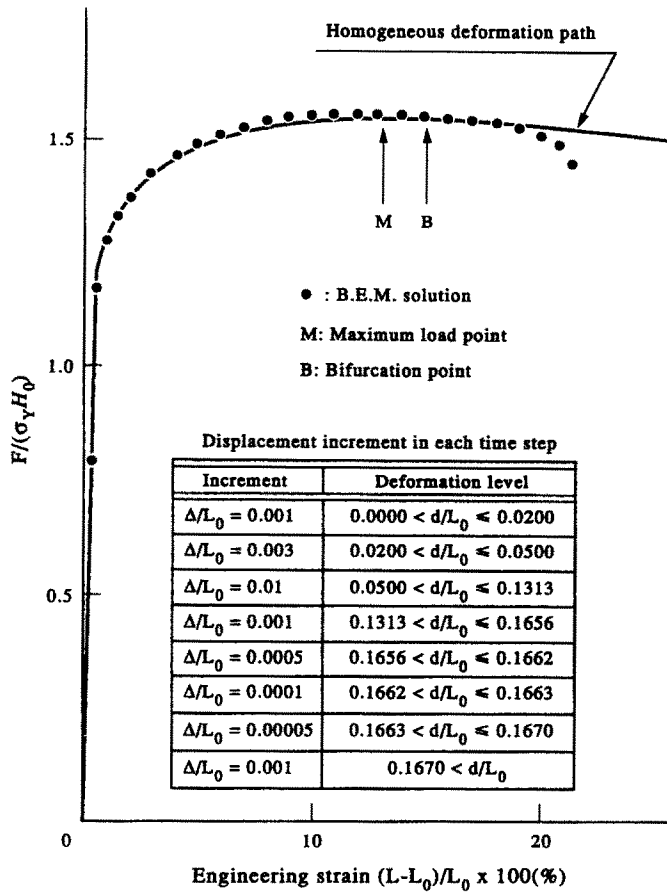


Fig. 19. Normalized load-engineering strain curve for the case 2 (Analysed by present full tangent stiffness field-boundary element approach.)

is  $\frac{1}{3}$ , as shown in Figs 24(a), (b) and (c) wherein the distribution of  $\bar{\epsilon}^P$  is illustrated at the engineering strains 16.6%, 17.2% and 20.7%. In Fig. 25, the distribution of  $\bar{\epsilon}^P$  at the engineering strain 20.7% is shown. When the finite element method was used for a problem of this class [see, for instance, McMeeking and Rice (1975)], geometric imperfections were often introduced into the problem to lead the analysis automatically into a diffused necking mode of deformation. When the initial imperfections are considered to be absent, a superposition of a small magnitude of the necking mode (with elastic unloading at the top of the bar) onto the homogeneous deformation mode, we found to be necessary when the finite element method is used in Murakawa and Atluri (1980), to lead the tensile bar into the region of diffuse necking. But, in the present full tangent stiffness field-boundary element analysis, the initial geometric imperfection is not introduced into the problem. Since all the effects of non-linearities in the problem are properly and directly accounted for the calculation of the velocity (displacement) field, the present full tangent stiffness field-boundary element analysis is quite sensitive to numerical instabilities. The diffused necking instability contained in the problem is propagated by the effect of a small amount of numerical error produced in numerical integrations, which makes the present algorithm switch its solution path from the fundamental homogeneous mode to the diffused necking mode by itself. The analysis is quite sensitive to the time increment in the incremental elastic-plastic analysis, when the numerical instabilities are propagating in the problem. Hence, this necessitates the time increment in each time step to be controlled† very carefully around the bifurcation

† It is well known that the determinant of the tangent stiffness matrix changes its sign when the deformation path passes through the bifurcation necking point. Thus, the determinant of the tangent stiffness is carefully maintained at each increment. If a change in its sign is detected the size of the increment is reduced, and then carefully controlled, to precisely define the bifurcation point, as well as the post-bifurcation necking solution.



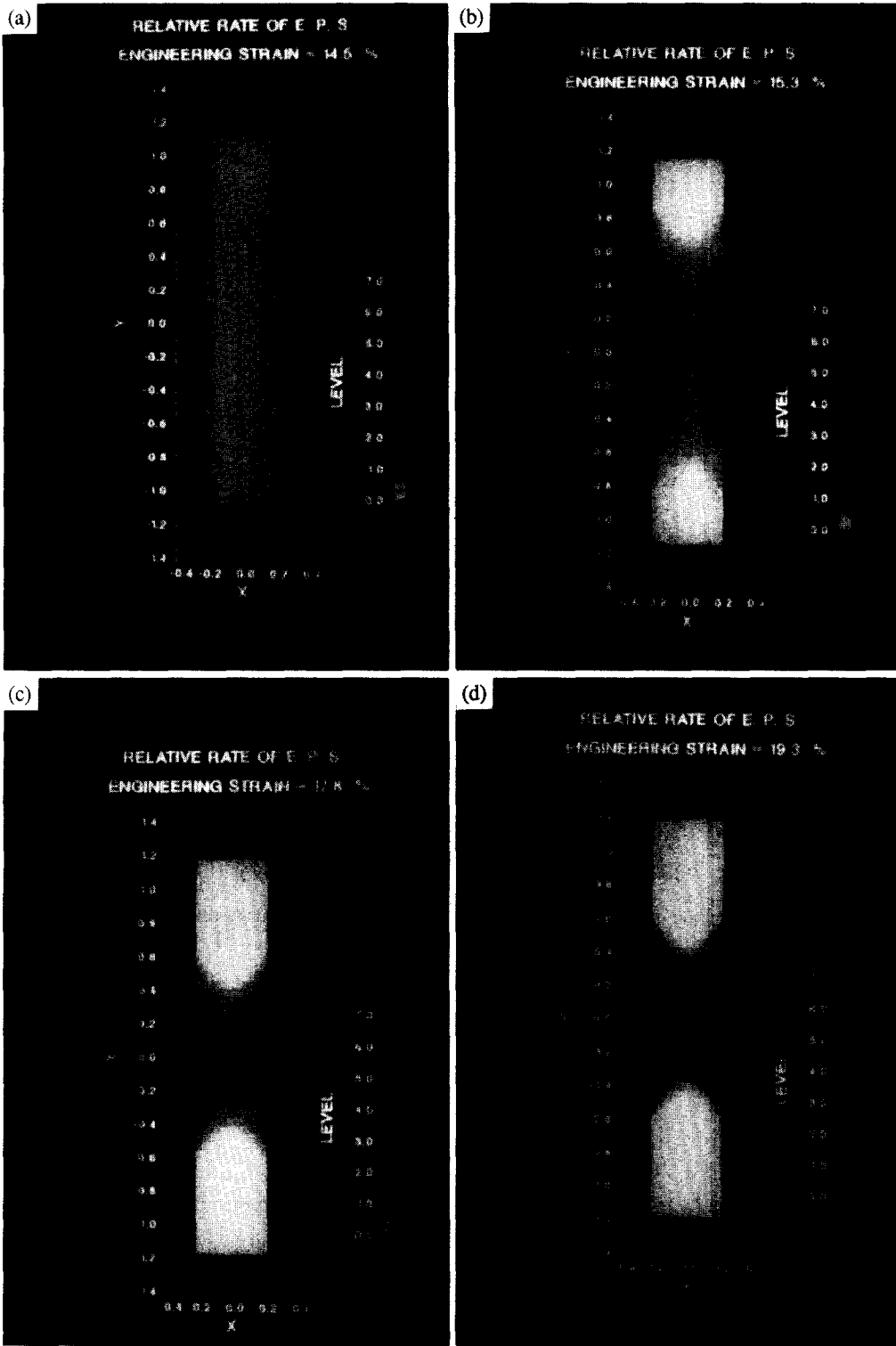


Fig. 22. Distributions of the relative rate of equivalent plastic strain for the case 1, at the engineering strain (a) 14.5%, (b) 15.3%, (c) 17.8% and (d) 19.3%.

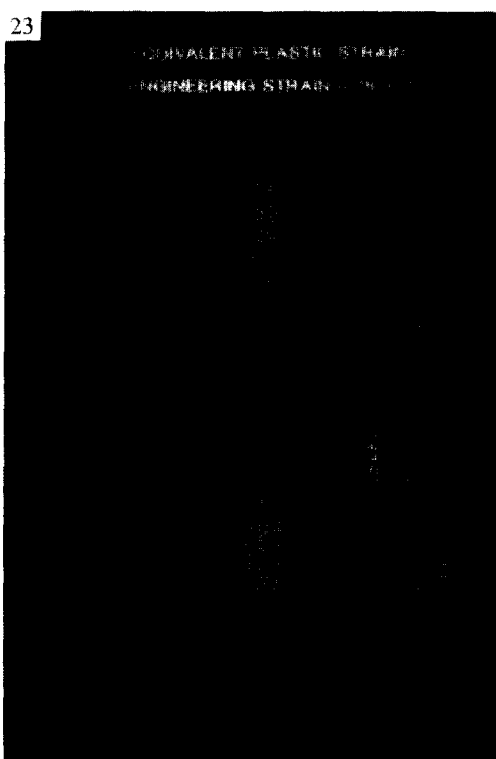


Fig. 23. Distribution of equivalent plastic strain for the case 1, at the engineering strain 19.3%.

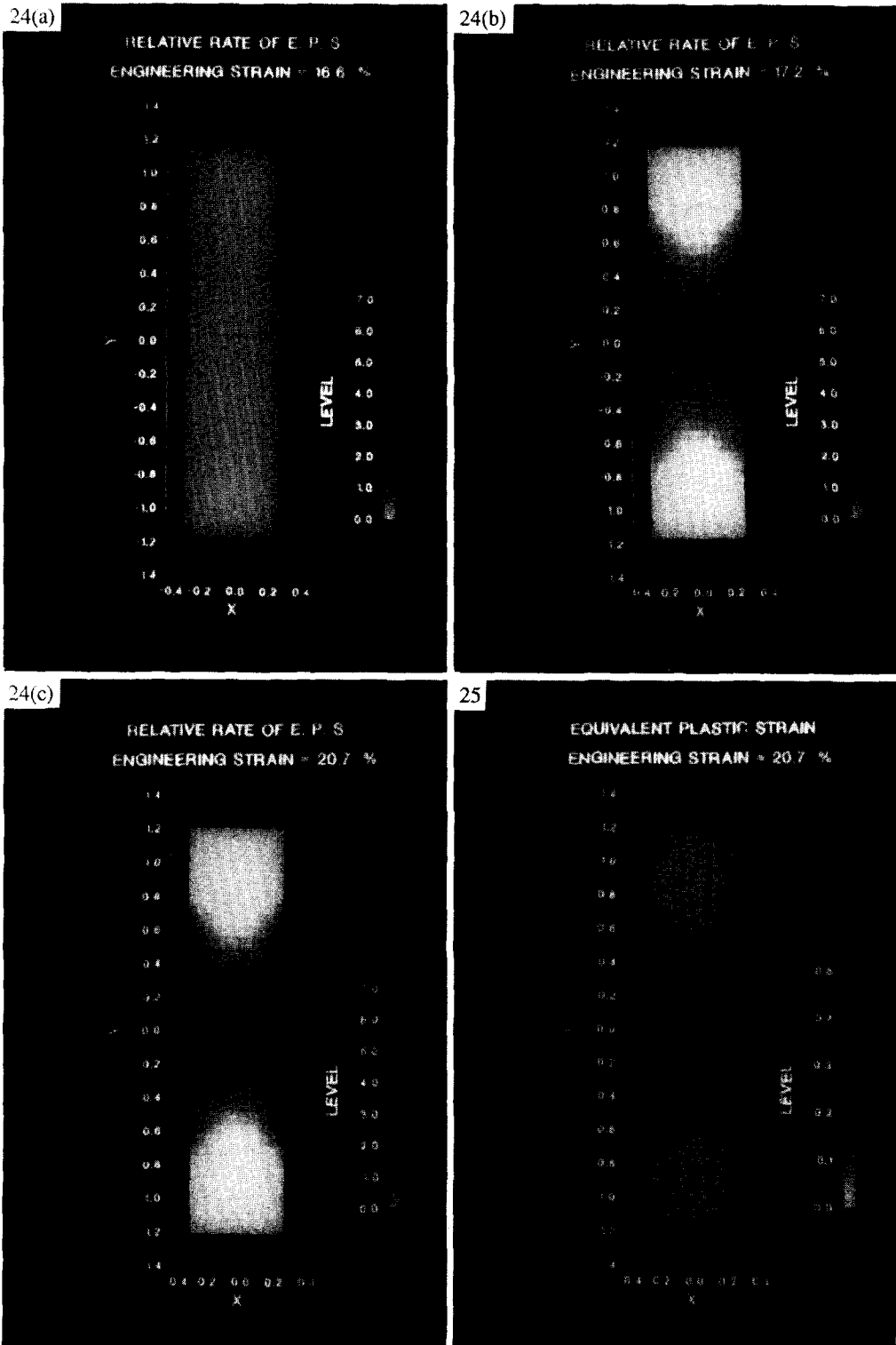


Fig. 24. Distributions of the relative rate of equivalent plastic strain for the case 2, at the engineering strain (a) 16.6%, (b) 17.2%, (c) 20.7%.

Fig. 25. Distribution of equivalent plastic strain for the case 2, at the engineering strain 20.7%.



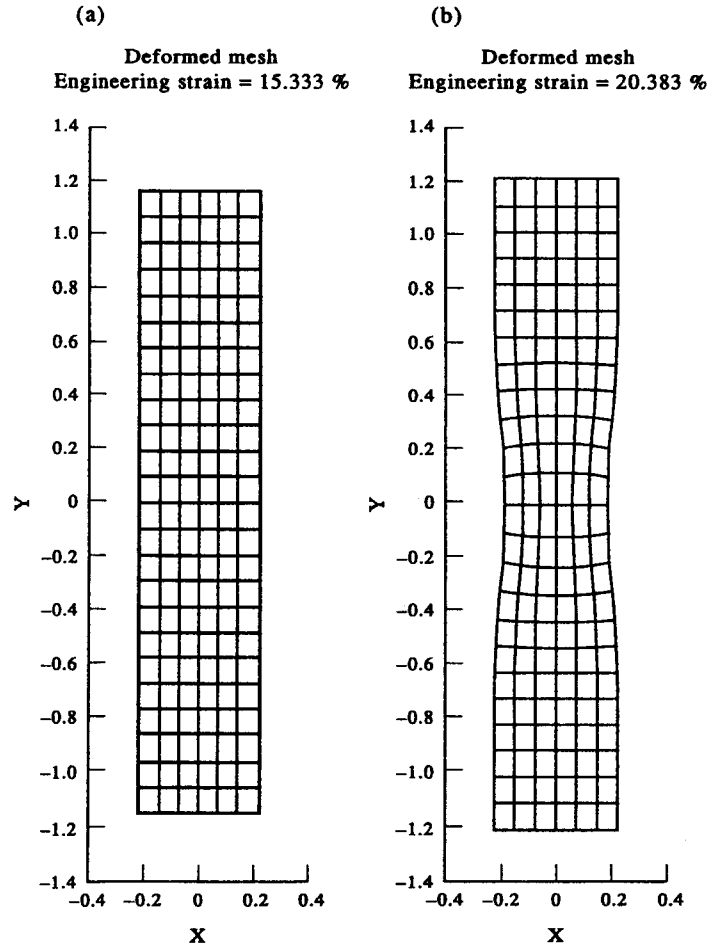


Fig. 20(a). Deformed mesh configurations for the case 1, at the engineering strain 15.3% ;  
(b) at the engineering strain 20.4%.

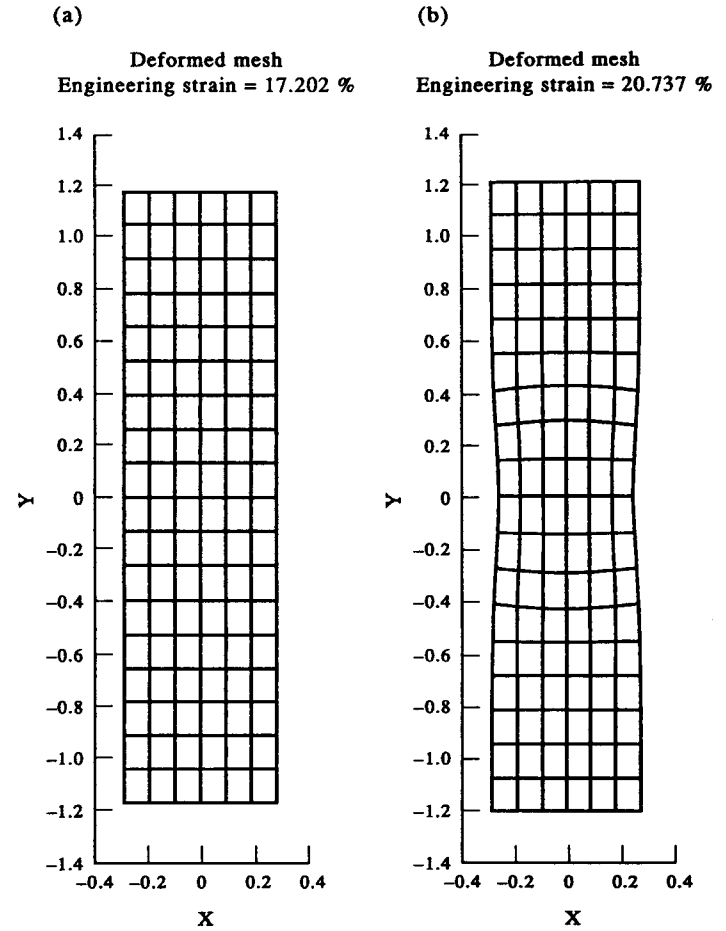


Fig. 21(a). Deformed mesh configurations for the case 2, at the engineering strain 17.2% ;  
(b) at the engineering strain 20.7%.

point. If the time increment is too large, then the analysis would ignore the numerical instabilities around the bifurcation point, and trace over the fundamental homogeneous deformation path.

As described above, the present full tangent stiffness field-boundary element method is superior to the conventional approach using an initial strain iteration algorithm, in capturing plastic instabilities. Moreover, as shown in this section, the present approach is capable not only of capturing the plastic instability but also of analysing the post bifurcation behavior. The solution algorithm presented here is based on a full tangent stiffness field-boundary element method where the velocity field both inside and on the boundary of the body is taken as the primary variable. Such a scheme takes the initial stress velocity gradient coupling terms accurately into account (unlike the conventional initial strain type algorithm). This is of paramount importance to these geometric and material non-linear instability problems. It has also been shown that such an algorithm is also capable of analysing the post-bifurcation behavior.

*Acknowledgements*—The support for this work from ONR, and the encouragement of Dr Y. Rajapakse, are gratefully appreciated. The collaboration of Dr H. Rajiyah in the course of study on BEM is thankfully acknowledged.

#### REFERENCES

- Atluri, S. N. (1979). On rate principles for finite strain analysis of elastic and inelastic analysis. In *Recent Research on Mechanical Behavior of Solids*, pp. 79–107. University of Tokyo Press, Tokyo.
- Atluri, S. N. (1980). On some new general and complementary energy theorems for the rate problems of finite strain, classical elastoplasticity. *J. Struct. Mech.* **8**, 61–92.
- Atluri, S. N. (1984a). On constitutive relations at finite strain hypo-elasticity and elasto-plasticity with isotropic or kinematic hardening. *Comp. Meth. Appl. Mech. Engng* **43**, 137–171.
- Atluri, S. N. (1984b). Computational solid mechanics (finite elements and boundary elements): present status and future directions. *Proc. 4th Int. Conf. on Applied Numerical Modelling* (Edited by H. M. Hsia *et al.*), pp. 19–37.
- Atluri, S. N. (1985). Notes and comments on computational elastoplasticity: some new models and their numerical implementation. *Proc. Finite Elements in Computational Mechanics* (Edited by T. Kant), pp. 271–289. Pergamon Press.
- Banerjee, P. K. and Butterfield, R. (1981). *Boundary Element Methods in Engineering Science*. McGraw-Hill, London and New York.
- Banerjee, P. K. and Cathie, D. N. (1980). A direct formulation and numerical implementation of the boundary element method for two-dimensional problems of elastoplasticity. *Int. J. Mech. Sci.* **22**, 233–245.
- Banerjee, P. K. and Raveendra, S. T. (1986). Advanced boundary element analysis of two- and three-dimensional problems of elasto-plasticity. *Int. J. Numer. Meth. Engng* **23**, 985–1002.
- Banerjee, P. K. and Raveendra, S. T. (1987). New boundary element formulation for two-dimensional elastoplastic analysis. *J. Engng Mech.* **113**, 252–265.
- Brebbia, C. A. (1978). *The Boundary Element Method in Engineering*. Pentech Press, London.
- Chandra, A. and Mukherjee, S. (1983). Applications of the boundary element method to large strain large deformation problems of viscoplasticity. *J. Strain Anal.* **18**, 261–270.
- Cruse, T. A. (1969). Numerical solutions in three-dimensional elastostatics. *Int. J. Solids Structures* **5**, 1259–1274.
- Guiggiani, M. and Casalini, P. (1987). Direct computation of Cauchy principal value integrals in advanced boundary elements. *Int. J. Numer. Meth. Engng* **24**, 1711–1720.
- Guiggiani, M. and Gigante, A. (1990). A general algorithm for multidimensional Cauchy principal value integrals in the boundary element method. *J. Appl. Mech.* **57**, 906–915.
- Im, S. and Atluri, S. N. (1987a). A study of two finite strain plasticity models: an internal time theory using Mandel's director concept, and a general isotropic/kinematic hardening theory. *Int. J. Plast.* **3**, 163–191.
- Im, S. and Atluri, S. N. (1987b). Endochronic constitutive modeling of finite deformation plasticity and creep: a field-boundary element computational algorithm. In *Recent Advances in Computational Methods for Inelastic Stress Analysis* (Edited by S. Nakazawa and K. Williams) ASME.
- Krishnasamy, G., Rizzo, F. J. and Rudolph, T. J. (1991). Hypersingular boundary integral equations: Their occurrence, interpretation, regularization and computation. In *Developments in Boundary Element Methods* (Edited by P. K. Banerjee and S. Kobayashi), Advanced Dynamic Analysis, Vol. 7, Chapter 7, Elsevier Applied Science Publishers.
- Lachat, J. C. and Watson, J. O. (1976). Effective numerical treatment of boundary integral equations: a formulation for three-dimensional elastostatics. *Int. J. Numer. Meth. Engng* **10**, 991–1005.
- Lee, E. H., Mallett, R. L. and Wertheimer, T. B. (1983). Stress analysis for anisotropic hardening in finite deformation plasticity. *ASME J. Appl. Mech.* **50**, 554–560.
- McMeeking, R. M. and Rice, J. R. (1975). Finite-element formulation for problems of large elastic-plastic deformation. *Int. J. Solids Structures* **11**, 601–616.
- Mukherjee, S. (1977). Corrected boundary-integral equations in planar thermoelastoplasticity. *Int. J. Solids Structures* **13**, 331–335.
- Mukherjee, S. and Chandra, A. (1987). Nonlinear formulations in solid mechanics. In *Boundary Element Methods in Mechanics* (Edited by D. E. Beskos), pp. 286–331. Elsevier Science Publishers.

- Mukherjee, S. and Kumar, V. (1978). Numerical analysis of time-dependent inelastic deformation in metals. *ASME J. Appl. Mech.* **45**, 785–790.
- Murakawa, H. and Atluri, S. N. (1980). New general and complementary energy theorems finite strain rate inelasticity and finite elements. *Nonlinear Finite Element Analysis in Structural Mechanics* (Edited by Wunderlich, Stein and Bathe), pp. 29–47. Springer-Verlag.
- O'Donoghue, P. E. and Atluri, S. N. (1987). Field/boundary element approach to the large deflections of thin plates. *Comput. Struct.* **27**, 427–435.
- Okada, H., Rajiyah, H. and Atluri, S. N. (1988a). A novel displacement gradient boundary element methods for elastic stress analysis with high accuracy. *J. Appl. Mech.* **55**, 786–794.
- Okada, H., Rajiyah, H. and Atluri, S. N. (1988b). Some recent developments in finite-strain elastoplasticity using the field-boundary element method. *Comput. Struct* **30**, 275–288.
- Okada, H., Rajiyah, H. and Atluri, S. N. (1989). Non-hyper singular integral representations for velocity (displacement) gradients in elastic/plastic solids (small or finite deformations). *Comput. Mech.* **4**, 165–175.
- Okada, H., Rajiyah, H. and Atluri, S. N. (1990). A full tangent stiffness field-boundary-element formulation for geometric and material non-linear problems of solid mechanics. *Int. J. Numer. Meth. Engng.* **29**, 15–35.
- Reed, K. W. and Atluri, S. N. (1983). Analysis of large quasistatic deformations of inelastic bodies by a new hybrid-stress finite element algorithm. *Comput. Meth. Appl. Mech. Engng* **39**, 245–295.
- Reed, K. W. and Atluri, S. N. (1985). Constitutive modeling and computational implementation for finite strain plasticity. *Int. J. Plast.* **1**, 63–87.
- Rizzo, A. (1967). An integral equation approach to boundary value problems in classical elastostatics. *Q. Appl. Math.* **25**, 83–95.
- Rubinstein, R. and Atluri, S. N. (1983). Objectivity of incremental constitutive relations over finite time steps in computational finite deformation analysis. *Comput. Meth. Appl. Mech. Engng* **36**, 277–290.
- Stroud, A. H. (1966). *Gaussian Quadrature Formulas*. Prentice-Hall Inc.
- Stroud, A. H. (1971). *Approximate Calculation of Multiple Integrals*. Prentice-Hall Inc.
- Swedlow, J. L. and Cruse, T. A. (1971). Formulation of boundary integral equations for three-dimensional elastoplastic flow. *Int. J. Solids Structures* **7**, 1673–1683.
- Watanabe, O. and Atluri, S. N. (1986a). Internal time, general internal variable, and multiyield surface theories of plasticity and creep: a unification of concepts. *Int. J. Plast.* **2**, 107–134.
- Watanabe, O. and Atluri, S. N. (1986b). Constitutive modeling of cyclic plasticity and creep, using an internal time concept. *Int. J. Plast.* **2**, 107–134.
- Zhang, J.-D. and Atluri, S. N. (1986). A boundary/interior element method for quasistatic and transient response analysis of shallow shells. *Comput. Struct.* **24**, 213–224.